

Climate extremes indices in the CMIP5 multimodel ensemble: Part 2. Future climate projections

J. Sillmann,¹ V. V. Kharin,¹ F. W. Zwiers,² X. Zhang,³ and D. Bronaugh²

Received 5 July 2012; revised 1 November 2012; accepted 1 November 2012; published 25 March 2013.

[1] This study provides an overview of projected changes in climate extremes indices defined by the Expert Team on Climate Change Detection and Indices (ETCCDI). The temperature- and precipitation-based indices are computed with a consistent methodology for climate change simulations using different emission scenarios in the Coupled Model Intercomparison Project Phase 3 (CMIP3) and Phase 5 (CMIP5) multimodel ensembles. We analyze changes in the indices on global and regional scales over the 21st century relative to the reference period 1981–2000. In general, changes in indices based on daily minimum temperatures are found to be more pronounced than in indices based on daily maximum temperatures. Extreme precipitation generally increases faster than total wet-day precipitation. In regions, such as Australia, Central America, South Africa, and the Mediterranean, increases in consecutive dry days coincide with decreases in heavy precipitation days and maximum consecutive 5 day precipitation, which indicates future intensification of dry conditions. Particularly for the precipitation-based indices, there can be a wide disagreement about the sign of change between the models in some regions. Changes in temperature and precipitation indices are most pronounced under RCP8.5, with projected changes exceeding those discussed in previous studies based on SRES scenarios. The complete set of indices is made available via the ETCCDI indices archive to encourage further studies on the various aspects of changes in extremes.

Citation: Sillmann, J., V. V. Kharin, F. W. Zwiers, X. Zhang, and D. Bronaugh (2013), Climate extremes indices in the CMIP5 multimodel ensemble: Part 2. Future climate projections, *J. Geophys. Res. Atmos.*, 118, 2473–2493, doi:10.1002/jgrd.50188.

1. Introduction

[2] Extreme climate events and their changes are of particular relevance to society and ecosystems due to their potentially severe impacts as emphasized in the Special Report on Extreme Events (SREX) of the Intergovernmental Panel on Climate Change [IPCC, 2012]. Correspondingly, the demand for consistent and robust projections of future changes in climate extremes has rapidly increased over the past decade. To facilitate the investigation of observed and projected changes, particularly in temperature and precipitation extremes, the Expert Team on Climate Change Detection and Indices (ETCCDI) defined a set of climate change indices focusing on extreme events. These indices in general describe moderate extreme events with a re-occurrence time of 1 year

or less, forming a balance between data availability and robustness of changes [Zhang *et al.*, 2011].

[3] The ETCCDI climate change indices, simply referred to as indices in the following, have been widely used for analyzing global changes in extremes in observational records [e.g., Frich *et al.*, 2002; Kiktev *et al.*, 2003; Alexander *et al.*, 2006] as well as in future climate projections [e.g., Tebaldi *et al.*, 2006; Sillmann and Roeckner, 2008; Orlowsky and Seneviratne, 2012]. In the guidelines of the World Meteorological Organization (WMO) on the analysis of extremes in a changing climate [Klein Tank *et al.*, 2009], it is further pointed out that “Projected changes in the indices are indicative of future climate change in extremes. By using the same definitions of extremes and analyzing the data in a standardized way, it is possible to compare results from different places and to obtain coherent pictures of change around the world.”

[4] Another important contribution toward consistent future projections of changes in extremes are the efforts of the Coupled Model Intercomparison Project Phase 3 (CMIP3) [Meehl *et al.*, 2007b] and Phase 5 (CMIP5) [Taylor *et al.*, 2012], which provide coordinated simulations from state-of-the-art global climate models. Multimodel ensemble simulations have been shown to outperform individual models and are also expected to provide more robust estimates of future changes and model related uncertainties [e.g., Gleckler *et al.*, 2008; Sillmann *et al.*, 2013]. CMIP5 features substantial model improvements compared to CMIP3

All supporting information may be found in the online version of this article.

¹Canadian Centre for Climate Modelling and Analysis, Victoria, British Columbia, Canada.

²Pacific Climate Impacts Consortium, Victoria, British Columbia, Canada.

³Environment Canada, Toronto, Ontario, Canada.

Corresponding author: J. Sillmann, Canadian Centre for Climate Modelling and Analysis, University of Victoria, Victoria, BC, Canada. (jana.sillmann@ec.gc.ca)

©2013. American Geophysical Union. All Rights Reserved.
2169-897X/13/10.1002/jgrd.50188

[*Taylor et al.*, 2012] and utilizes a new set of emission scenarios referred to as Representative Concentration Pathways (RCPs) [*Moss et al.*, 2010; *van Vuuren et al.*, 2011b]. The future climate simulations of the CMIP3 ensemble were based on the emission scenarios described in the IPCC Special Report on Emission Scenarios (SRES) [*Nakicenovic et al.*, 2000].

[5] Beside the different emission scenarios and models, differences in the index calculations themselves can also lead to inconsistencies in the analysis and comparison of changes in extremes simulated in the CMIP3 and CMIP5 ensembles. For instance, *Tebaldi et al.* [2006] used indices that were provided as part of CMIP3 by individual model groups using their own implementations of index calculations, which can lead to inconsistencies. *Orlowsky and Seneviratne* [2012] used a larger suite of CMIP3 simulations to calculate a set of indices, which deviated slightly from the ETCCDI definitions.

[6] The purpose of this study is thus to document changes in indices that are calculated in a consistent manner as simulated in the CMIP3 and CMIP5 multimodel ensembles for different emission scenarios. As shown in *Rogelj et al.* [2012], the radiative forcing prescribed in the SRES and RCP scenarios can lead to different average temperature responses, and we expect that this will also be evident in seasonal and annual temperature and precipitation extremes.

[7] As an essential part of this study, an ETCCDI indices archive (EIA) of indices for the CMIP3 and CMIP5 ensembles has been created and is available at <http://www.cccma.ec.gc.ca/data/climdex/climdex.shtml>. The EIA is described in detail in part 1 of this study [*Sillmann et al.*, 2013], which focuses on the evaluation of the indices in CMIP3 and CMIP5 under present climate conditions. With the exception of a few indices, we show in *Sillmann et al.* [2013] that CMIP5 models are generally able to simulate climate extremes and their trend patterns as represented by the indices in comparison to a gridded observational indices data set. The challenges involved in such an evaluation, given the temporal and spatial resolution of GCMs as well as the availability of suitable observational data sets, are also discussed. Part 2 of this study, which is presented here, focuses on the projected changes in the indices based on CMIP3 and CMIP5 future climate simulations.

[8] The paper is organized as follows. We briefly describe the multimodel ensembles and featured scenarios in section 2. In section 3, we provide the definitions of indices discussed in this paper. Our results are presented in section 4 for several different categories of temperature- and precipitation-based indices. A summary of the main findings and concluding remarks are given in section 5.

2. Climate Models and Scenarios

[9] We analyze climate simulations of the 20th and 21st century performed by models participating in CMIP3 [*Meehl et al.*, 2007b] and CMIP5 [*Taylor et al.*, 2012]. While more than one realization is available for some models, we analyze here only the first ensemble member of each model simulation as a first-order assessment. The CMIP3 and CMIP5 model output is available from the data archives of the Program for Climate Model Diagnosis and Intercomparison (PCMDI, <http://www-pcmdi.llnl.gov>) and the Earth System Grid data distribution portal (ESG, <http://www.earthsystemgrid.org>). At the time of

writing, we were able to analyze 19 CMIP5 models (cf. Table 1), for which daily model output for three RCP scenarios (RCP2.6, 4.5 and 8.5) was available. However, the indices for all CMIP5 models on the ESG are being made available on the EIA (<http://www.cccma.ec.gc.ca/data/climdex/climdex.shtml>) for further analysis. We also analyze 11 CMIP3 models (see Table 2), for which the three SRES emission scenarios considered here (B1, A1B, and A2) are available in the PCMDI archive. Note that the models used in this study differ from the models in *Tebaldi et al.* [2006], who use fewer models, and *Orlowsky and Seneviratne* [2012], who use more models but only for the SRES A2 scenario.

[10] Figure 1 illustrates the evolution of carbon dioxide (CO₂) concentrations as observed in the 20th century and prescribed in the 21st century simulations in the SRES and RCP scenarios considered in this study. The SRES scenarios are based on storylines assuming different socioeconomic, technological, and political developments leading to specified changes in emissions that in turn determine the resulting changes in atmospheric greenhouse gas concentrations (e.g., Figure 1) and radiative forcing. At the end of the 21st century, the CO₂ concentrations reach about 840 ppm in the SRES A2 scenario, 700 ppm in the A1B scenario, and 540 ppm in the B1 scenario which assumes the most environmentally friendly development pathway.

[11] In contrast to the SRES scenarios, the radiative forcing trajectories in the RCPs are not associated with predefined storylines and can reflect various possible combinations of economic, technological, demographic, and policy developments [*Moss et al.*, 2010]. The peak-and-decline RCP2.6 scenario is designed to meet the 2°C global average warming target compared to pre-industrial conditions [*van Vuuren et al.*, 2011a]. It has a peak in the radiative forcing at approximately 3 W/m² (~400 ppm CO₂) before 2100 and then declines to 2.6 W/m² by the end of the 21st century (~330 ppm CO₂, Figure 1). Radiative forcing in RCP4.5 peaks at about 4.5 W/m² (~540 ppm CO₂) in year 2100 [*Thomson et al.*, 2011]. RCP4.5 is comparable to the SRES scenario B1 with similar CO₂ concentrations and median temperature increases by 2100 according to *Rogelj et al.* [2012]. RCP8.5 assumes a high rate of radiative forcing increase, peaking at 8.5 W/m² (~940 ppm CO₂) in year 2100 [*Riahi et al.*, 2011].

[12] Climate changes simulated in the CMIP3 and CMIP5 ensembles are not directly comparable because of the differences in prescribed forcing agents (e.g., CO₂ and aerosols) between the SRES and RCP scenarios as discussed in *Rogelj et al.* [2012]. Furthermore, the models may respond differently to a specific radiative forcing due to different model-specific climate sensitivities. However, based on the underlying radiative forcing (or CO₂ concentrations), one can compare projected changes in the temperature and precipitation indices and provide an estimate of uncertainty related to the different emission scenarios.

3. Global Climate Extremes Indices

[13] The indices are based on daily minimum and maximum of near surface temperature and daily precipitation amounts (TN, TX, and PR, respectively). Detailed information on the

Table 1. The CMIP5 Models for Which RCP2.6, RCP4.5 and RCP8.5 Simulations Where Available on the ESG (as of September 2012) for the Time Period 2006–2100^a

| | Model | Institution | Spatial Resolution (Lon × Lat~Levels) |
|----|----------------|--|---------------------------------------|
| 1 | BCC-CSM1-1 | Beijing Climate Center, China Meteorological Administration, China | 128 × 64L26(T42) |
| 2 | BNU-ESM | Beijing Normal University, China | 128 × 64L26(T42) |
| 3 | CanESM2 | Canadian Centre for Climate Modelling and Analysis, Canada | 128 × 64L35(T63) |
| 4 | CCSM4 | National Center for Atmospheric Research (NCAR), USA | 288 × 192L26 |
| 5 | CNRM-CM5 | Centre National de Recherches Meteorologiques, Meteo-France, France | 256 × 128L31(T127) |
| 6 | CSIRO-Mk3-6-0 | Australian Commonwealth Scientific and Industrial Research Organization, Australia | 192 × 96L18(T63) |
| 7 | FGOALS-s2 | Institute of Atmospheric Physics, Chinese Academy of Sciences, China | 128 × 108L26 |
| 8 | GFDL-ESM2G | Geophysical Fluid Dynamics Laboratory, USA | 144 × 90L24 |
| 9 | GFDL-ESM2M | Geophysical Fluid Dynamics Laboratory, USA | 144 × 90L24 |
| 10 | HadGEM2-ES | Met Office Hadley Centre, UK | 192 × 145L40 |
| 11 | IPSL-CM5A-LR | Institut Pierre-Simon Laplace, France | 96 × 96L39 |
| 12 | IPSL-CM5A-MR | Institut Pierre-Simon Laplace, France | 144 × 143L39 |
| 13 | MIROC5 | AORI (Atmosphere and Ocean Research Institute), NIES (National Institute for Environmental Studies), JAMSTEC (Japan Agency for Marine-Earth Science and Technology), Japan | 256 × 128L40(T85) |
| 14 | MIROC-ESM | AORI, NIES, JAMSTEC, Japan | 128 × 64L80(T42) |
| 15 | MIROC-ESM-CHEM | AORI, NIES, JAMSTEC, Japan | 128 × 64L80(T42) |
| 16 | MPI-ESM-LR | Max Planck Institute for Meteorology, Germany | 192 × 96L47(T63) |
| 17 | MPI-ESM-MR | Max Planck Institute for Meteorology, Germany | 192 × 96L95(T63) |
| 18 | MRI-CGCM3 | Meteorological Research Institute, Japan | 320 × 160L48(T159) |
| 19 | NorESM1-M | Norwegian Climate Centre, Norway | 144 × 96L26 |

^aNote that all three RCP simulations of BCC-CSM1-1 as well as the RCP8.5 simulation on HadGEM2-ES were only available until year 2099. The analysis reported in this paper is based on the first ensemble member of each RCP simulation.

Table 2. The CMIP3 Models for Which All SRES Scenarios (i.e., B1, A1B, and A2) Where Available on the PCMDI Archive

| | Model | Institution | Spatial resolution (Lon × Lat~Levels) |
|----|-----------------|--|---------------------------------------|
| 1 | ccma-cgcm3 t47 | Canadian Centre for Climate Modelling and Analysis, Canada | 96 × 48L32 (T47) |
| 2 | ccma-cgcm3 t63 | Canadian Centre for Climate Modelling and Analysis, Canada | 128 × 64L32 (T63) |
| 3 | crrm-cm3 | Centre National de Recherches Meteorologiques, Meteo-France, France | 128 × 64L45 (T63) |
| 4 | csiro-mk3-0 | Australian Commonwealth Scientific and Industrial Research Organization, Australia | 192 × 96L18 (T63) |
| 5 | csiro-mk3-5 | Australian Commonwealth Scientific and Industrial Research Organization, Australia | 192 × 96L18 (T63) |
| 6 | gfdl-cm2-0 | NOAA/Geophysical Fluid Dynamics Laboratory, USA | 144 × 90L24 |
| 7 | gfdl-cm2-1 | NOAA/Geophysical Fluid Dynamics Laboratory, USA | 144 × 90L24 |
| 8 | giiss-model-e-r | NASA/Goddard Institute for Space Studies, USA | 72 × 46L20 |
| 9 | ipsl-cm4 | Institut Pierre-Simon Laplace, France | 96 × 72L19 |
| 10 | miroc3-2 medres | CCSR/NIES/FRCGC, Japan | 128 × 64L20 (T42) |
| 11 | mpi-echam5 | Max Planck Institute for Meteorology, Germany | 192 × 96L31 (T63) |

indices can be found in Alexander *et al.* [2006], Klein Tank *et al.* [2009], and Zhang *et al.* [2011] and on the ETCCDI website. For the multimodel analysis presented in this paper, all indices are first computed on their native model grids and then re-gridded to a common $2.5^\circ \times 2.5^\circ$ grid. While daily TN, TX, and PR are only available for two 20 year time periods 2046–2065 and 2081–2100 in CMIP3, they are available for the entire time period from 2006 to 2100 for CMIP5.

3.1. Selection of Indices

[14] In this study, we consider a subset of the 27 indices (see Table 1 in Sillmann *et al.* [2013]) available in the

EIA. The selected indices, as described below, give a comprehensive overview of the projected changes in temperature and precipitation extremes across models and scenarios. While most indices are defined on an annual basis, a few are also available as monthly statistics or as continuous counts over the total data record and will be specified as such in the description below.

3.1.1. Temperature Indices

[15] • Absolute Indices

The minimum of TN (TNn) and maximum of TX (TXx) represent the coldest or hottest day of a year, season, or month, respectively. The annual temperature extremes are used in several studies to express the extreme

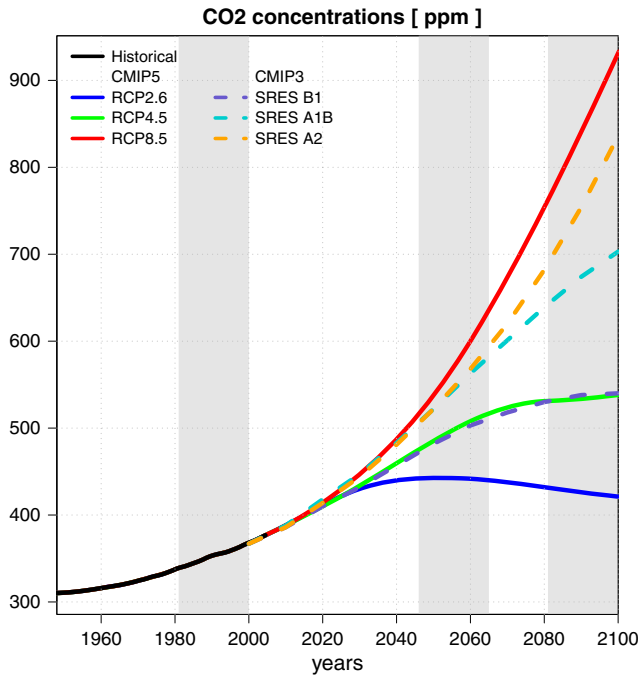


Figure 1. Carbon dioxide (CO₂) concentrations in ppm as used in the CMIP3 and CMIP5 historical and scenario simulations and available for download at the PCMDI website. The vertical shading indicates the reference period (1981–2000) and the two 20 year periods (2046–2065 and 2081–2100) considered in the analysis of future climate change.

temperature range, ETR [e.g., Alexander *et al.*, 2006; Tebaldi *et al.*, 2006] and to project future changes in 20 year return values of annual temperature extremes [e.g., Kharin *et al.*, 2007].

[16] • Threshold Indices

Frost days (FD) and tropical nights (TR) count the days when TN is below 0°C or above 20°C, respectively. These indices are often useful for climate impact studies. Changes in frost days, for instance, can be relevant for agricultural practice and engineering applications [e.g., Terando *et al.*, 2012]. Tropical nights usually occur in combination with extended periods of heat (particularly in extra-tropical regions) and have been suggested to be problematic for human health [e.g., Weisskopf *et al.*, 2002; Patz *et al.*, 2005].

[17] • Percentile Indices

The percentile indices are the exceedance rates (in %) above or below thresholds based on the annual cycle of the percentiles calculated for a 5 day sliding window centered on each calendar day in the base period, which is by definition 1961–1990. The calculation of the percentile thresholds in the base period includes a bootstrap resampling method [Zhang *et al.*, 2005] to avoid inhomogeneities at the beginning and end of the base period. In our analysis, we consider cold nights and days (TN10p and TX10p, respectively) and warm nights and days (TN90p and TX90p, respectively), which describe the threshold exceedance rate of days where TN or TX is below the 10th or above the 90th percentile, respectively.

[18] • Duration Indices

The warm and cold spell duration indices (WSDI and CSDI, respectively) are based on the percentile thresholds calculated from the base period 1961–1990 as described above. WSDI and CSDI count the number of days in a year when TX is above the 90th percentile for six consecutive days or longer, or when TN is below the 10th percentile for six consecutive days or longer, respectively. The advantage of using a percentile-based threshold instead of an absolute value threshold is that warm or cold spells can be captured for a wide variety of climatological conditions (e.g., tropics versus northern latitudes) as pointed out by Radinović and Ćurić [2012]. However, Orlowsky and Seneviratne [2012] found that this index is difficult to interpret in comparison with other heat wave indices.

3.1.2. Precipitation Indices

[19] • Absolute indices

The maximum 5 day precipitation index (RX5day) describes the monthly or annual maximum of 5 day precipitation accumulations. This index is often used to describe changes in potential flood risks as heavy rain conditions over several consecutive days can contribute to flood conditions [e.g., Frich *et al.*, 2002].

[20] • Threshold indices

The heavy precipitation days index (R10mm) counts the number of days with more than 10 mm of precipitation. This index is associated with the wet part of the precipitation distribution but does not generally describe extreme precipitation. Very wet days (R95p) describe the annual precipitation amount (in mm) accumulated on days when daily precipitation is greater than the 95th percentile threshold of the wet-day precipitation (PR > 1 mm) distribution derived from the base period, by definition, 1961–1990. As this index is based on a percentile threshold, it takes into account the respective precipitation climatologies of different regions.

[21] • Duration indices

The consecutive dry-day index (CDD) represents the length of the longest period of consecutive dry days (i.e., days with PR < 1 mm) in a year ending in that year. If a dry spell does not end in a particular year and spans a period longer than 1 year (as may happen in very dry regions), then CDD is not reported for that year and the accumulated dry days are carried forward to the year when the spell ends. This definition avoids the splitting of dry spells in regions where the dry season extends over the year boundary, in contrast to other studies such as Tebaldi *et al.* [2006] that use a CDD definition where dry spells are always terminated at the year's end. However, the definition used here can lead to problems in regions with very long dry spells, resulting in very large values at some grid points as noted in Sillmann *et al.* [2013]. CDD is the only ETCCDI index that describes the lower tail of the precipitation distribution and is often referred to as a drought indicator. As drought is a complex phenomenon depending on various other factors besides lack of precipitation, CDD can only provide an indication for meteorological drought and should be interpreted in combination with other precipitation indices [e.g., Tebaldi *et al.*, 2006; Orlowsky and Seneviratne, 2012] or drought indices [e.g., Cardona *et al.*, 2012].

[22] Two indices that do not fall in one of the categories outlined above are the total wet-day precipitation (PRCPTOT) and the simple daily intensity (SDII) indices. PRCPTOT describes the total annual amount of precipitation on wet days defined as days with more than 1 mm of precipitation. SDII describes the daily precipitation amount averaged over all wet days in a year. PRCPTOT and SDII are not necessarily associated with climate extremes but provide useful information about the relationship between changes in extreme conditions (e.g., RX5day or R95p) and other aspects of the distribution of daily precipitation.

4. Results

[23] The results are presented in terms of (1) the temporal evolution of spatially averaged indices for different RCPs from the mid-20th to the end of the 21st century, (2) the spatial patterns of changes for the time period 2081–2100, and (3) box-and-whisker plots that summarize regional and seasonal features of the projected changes, first for temperature indices and followed by precipitation indices. The changes are displayed relative to the 1981–2000 reference period which is common to both CMIP3 and CMIP5.

[24] Box-and-whisker plots represent the multimodel median, the interquartile model spread (i.e., the range between the 25th and 75th quantiles) and the full inter-model range. They are produced for 21 subregions as defined in Giorgi and Francisco [2000, cf. their Table 2] and shown here in Figure 2. The box-and-whisker plots summarize regional and temporal averages of annual and seasonal values over the considered future time period. The results are presented for the June-July-August (JJA) and December-January-February (DJF) seasons. Seasonal analysis is performed only for indices that are available on a monthly basis, such as the temperature-based percentile indices as well as TXx, TNn, and RX5day.

[25] As an aid to interpretation, the notional statistical significance of projected changes is evaluated using the non-parametric Wilcoxon signed-rank test [e.g., Wilks, 2006],

which tests whether the multimodel median change is zero. Changes that are not significant at the 5% significance level are indicated by stippling in the maps of projected changes. We do not consider inter-model agreement in the significance testing and stippling as in IPCC [2007], Tebaldi et al. [2006], and Orlowsky and Seneviratne [2012] and do not use any of the stippling conventions currently under discussion [e.g., Tebaldi et al., 2011; Power et al., 2012]. Instead, model agreement or disagreement is illustrated in terms of the interquartile model spread for the 21 subregions for a number of indices.

4.1. Temperature Indices

4.1.1. Absolute and Threshold Indices

4.1.1.1. Temporal Evolution

[26] We start our analysis with a comparison of CMIP3 and CMIP5 projections based on area-weighted global averages over land. Relative to the 1981–2000 reference period, there is a general increase in the annual minimum of TN (TNn, Figure 3a) and the annual maximum of TX (TXx, Figure 3b) over land in the 21st century. The increase in TNn is greater than that in TXx for all three CMIP5 RCPs. The multimodel median increase in TNn and TXx respectively over global land projected by the end of the 21st century is 1.8°C and 1.4°C in RCP2.6, 3.4°C and 2.7°C in RCP4.5, and 6.7°C and 5.4°C in RCP8.5. The simulated changes in TNn and TXx in CMIP3 for the SRES scenarios are indicated by the box-and-whisker plots and show a similar tendency of stronger warming in TNn than TXx. In the 2046–2065 period, the SRES A1B and A2 scenarios are comparable to RCP4.5 with an increase of 3°C in TNn and 2.5°C in TXx, whereas B1 is comparable to RCP2.6 with an increase of about 2°C in TNn and 1.5°C in TXx. By the end of the 21st century, B1 shows increases of approximately 3°C in TNn and 2.2°C in TXx, which are similar to the changes projected by the CMIP5 models in RCP4.5, particularly for TNn. CMIP3 A1B and A2 changes in TNn and TXx are within the range of those

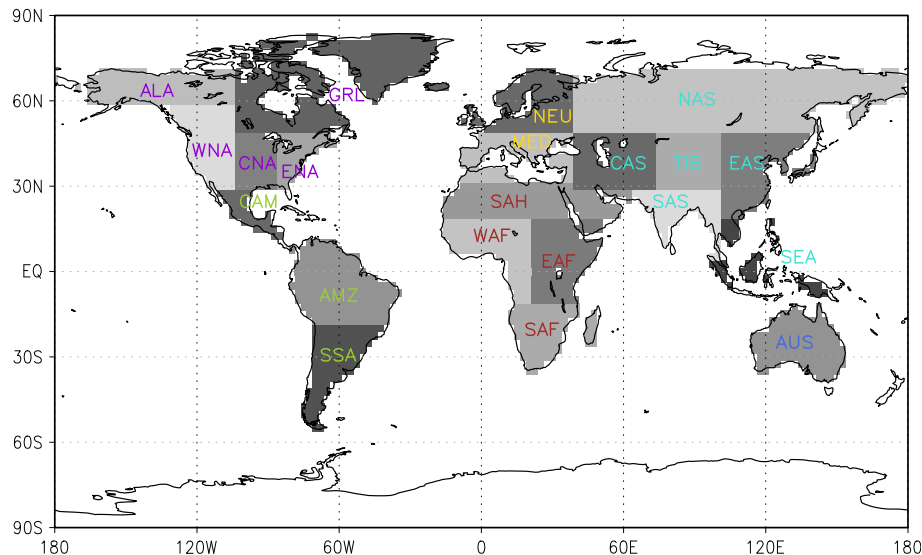


Figure 2. Subregions over land adapted from Giorgi and Francisco [2000, cf. their Table 2] and color-coded according to continents. Blue, Australia; green, South America; purple, North America; red, Africa; yellow, Europe; cyan, Asia.

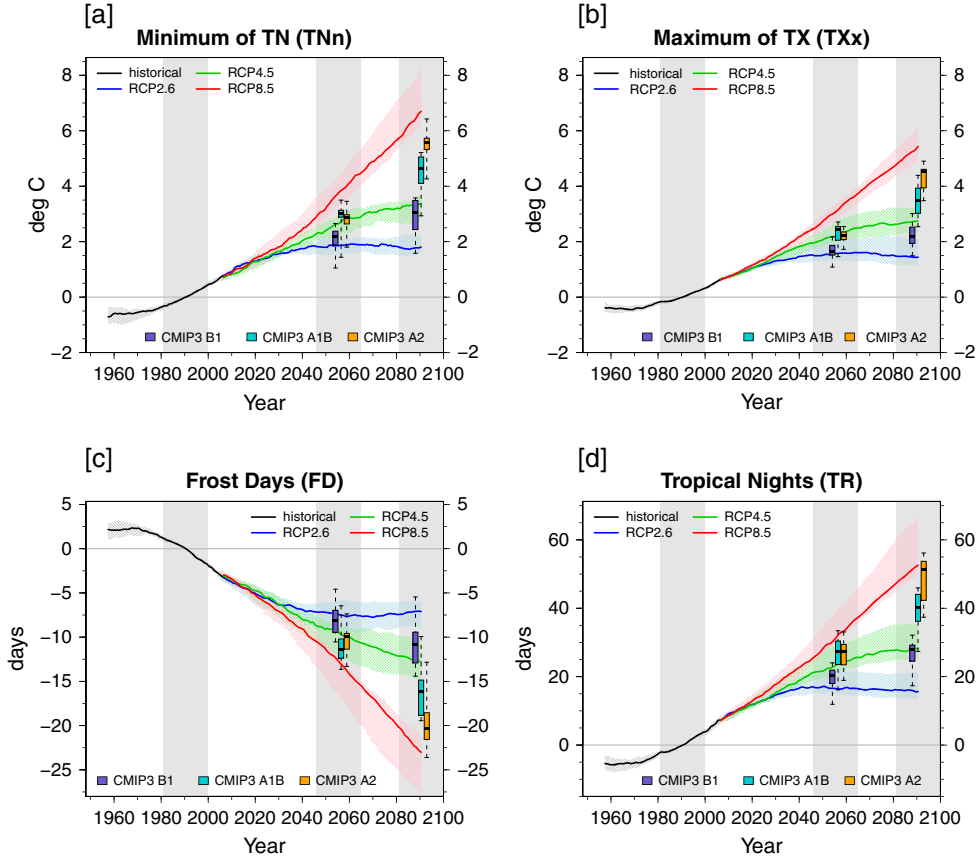


Figure 3. Global averages of temperature indices over land as simulated by the CMIP5 ensemble (see Table 1) for the RCP2.6 (blue), RCP4.5 (green), and RCP8.5 (red) displayed as anomalies from the reference period 1981–2000. Solid lines indicate the ensemble median and the shading indicates the interquartile ensemble spread (25th and 75th quantiles). Time series are smoothed with a 20 year running mean filter. The box-and-whisker plots show the interquartile ensemble spread (box) and outliers (whiskers) for 11 CMIP3 model simulations of the SRES scenarios A2 (orange), A1B (cyan), and B1 (purple) (see Table 2) globally averaged over the respective future time periods (2046–2065 and 2081–2100) as anomalies from the CMIP3 reference period 1981–2000.

simulated in CMIP5 for RCP4.5 and RCP8.5. TNn and TXx increase, respectively, by 4.6°C and 3.5°C in A1B, and by 5.6°C and 4.5°C in A2.

[27] A consistent pattern is seen in the evolution of the threshold indices based on TN, frost days (FD), and tropical nights (TR) globally averaged over land (Figures 3c and 3d). In the middle of the 21st century, FD decreases by about 8 days in B1, which lies in the interquartile model range of RCP2.6. FD decreases by 11 and 10 days in A1B and A2, respectively, which is within the interquartile model spread for RCP4.5. By the end of the 21st century, the median decreases of FD are 7 days in RCP2.6 and 13 days in RCP4.5, with B1 (10 days) being centered between them. A stronger decrease in FD of 16 and 20 days is seen in A1B and A2, respectively, which is still smaller than the median decrease of 23 days projected in RCP8.5.

[28] Tropical nights increase by about 18 days in RCP2.6 and 20 days in B1 in the middle of the 21st century. The A1B and A2 median increase of 27 days in TR is within the range of the projected RCP4.5 changes. At the end of the 21st century, the median TR increases most in RCP8.5 (53 days) closely followed by A2 (51 days) and A1B (40 days).

A modest median increase of 28 days is projected in RCP4.5 and B1. The smallest median increase in TR (16 days) is projected in the RCP2.6 scenario. The patterns in the temporal evolution of threshold indices based on daily maximum temperature such as ice days ($\text{TX} < 0^{\circ}\text{C}$) or summer days ($\text{TX} > 25^{\circ}\text{C}$) (not shown) are similar to those in FD and TR, respectively, but are less pronounced.

4.1.1.2. Spatial and Seasonal Patterns

[29] The projected median changes of TNn and TXx simulated in the CMIP5 ensemble are shown in Figure 4 and are significant across land areas for all three RCPs by the end of the 21st century. The spatial patterns of change in TNn and TXx are different. In particular, TNn increases more strongly in higher latitudes of the Northern Hemisphere. For RCP2.6, TXx changes only moderately over land while stronger increases are apparent in TNn, particularly in northern latitudes.

[30] The greatest changes in TNn, exceeding 12°C , are simulated in RCP8.5 in such regions as North America, Northern Europe, and North Asia. Presumably, larger changes in TNn in higher latitudes are related to the retreating snow cover under global warming whereas in the tropics and the Southern Hemisphere the TNn increases generally remain

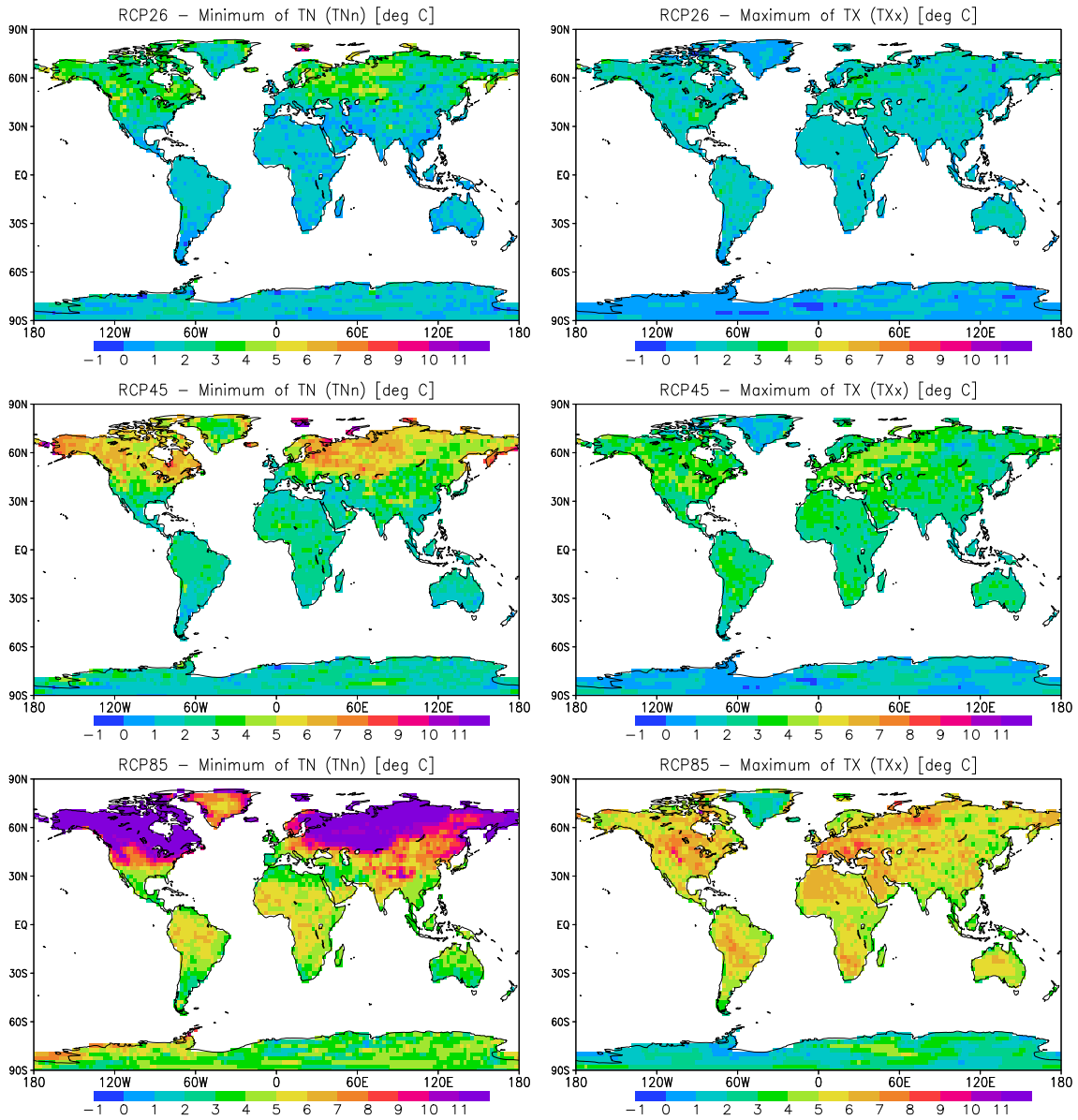


Figure 4. The multimodel median of temporally averaged changes in the minimum of TN (TNn, left) and the maximum of TX (TXx, right) over the time period 2081–2100 displayed as differences (in °C) relative to the reference period (1981–2000) for RCP2.6 (top), RCP4.5 (middle), and RCP8.5 (bottom). All changes are significant at the 5% significance level.

below 7°C and are comparable with those in TXx. The strongest warming in TXx generally occurs in the interior of the continents, such as in South and North America, Eastern Europe, north-central Eurasia as well as Australia.

[31] Regional summaries of the CMIP5 projected changes in 2081–2100 for the 21 subregions (cf. Figure 2) are depicted in Figure 5. The strongest median warming in TNn occurs in Alaska (ALA, 13°C) followed by that in Greenland (GRL) and Northern Europe (NEU) of about 11°C for RCP8.5. Strong warming in TNn can also be seen in West, Central, and East North America (WNA, CNA, and ENA, respectively), as well as North and Central Asia (NAS and CAS, respectively) and Tibet (TIB). In these regions, the increase in TNn is generally more pronounced in DJF (Figure 5e), whereas changes in JJA (Figure 5c) are more homogeneous across the regions.

[32] In contrast to TNn, TXx is projected to warm more uniformly over the land (Figure 5b). The maximum CMIP5 median increase of about 6.5°C in RCP8.5 occurs in WNA, CNA, ENA, MED, NEU, CAS, and NAS. The increases in TXx are generally more pronounced in JJA than DJF in all RCPs across the northern latitude regions (Figures 5d and 5f). The Mediterranean (MED) in particular is a region where the TXx warming of about 7°C in JJA for RCP8.5 is among the greatest across all subregions and exceeds the TNn warming of 6°C. In contrast, TNn and TXx increase only by about 4.5°C in DJF. That is, Mediterranean summer extreme temperatures warm more than winter extreme temperatures, whereas the opposite is generally true for the other subregions. The pronounced summer warming in MED may be related to soil moisture feedbacks [e.g., Hirschi et al., 2011] and precipitation deficits [Mueller and

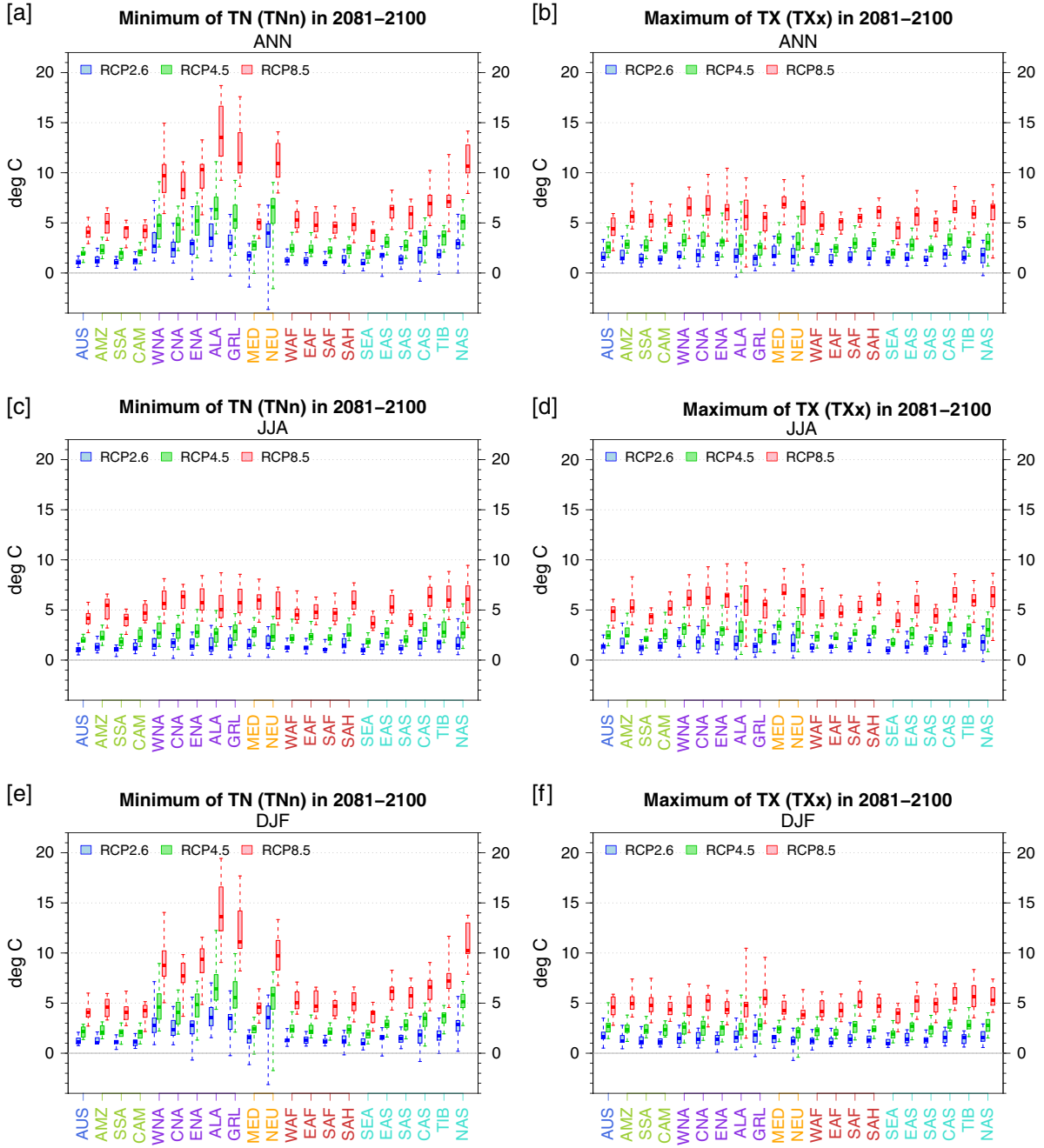


Figure 5. Projected changes (in $^{\circ}\text{C}$) in annual (ANN), JJA and DJF minima of TN (TNn, left) and maximum TX (TXx, right) over the time period 2081–2100 as differences relative to the reference period (1981–2000) for RCP2.6 (blue), RCP4.5 (green), and RCP8.5 (red). Regional mean changes are shown for each of the 21 subregions (cf. Figure 2). Boxes indicate the interquartile model spread (25th and 75th quantiles) with the horizontal line indicating the ensemble median and the whiskers showing the extreme range of the CMIP5 ensemble.

Seneviratne, 2012], which can play an important role in amplifying heat conditions.

[33] A similar pattern of seasonal and regional changes in TNn and TXx is seen for RCP4.5 and RCP2.6, albeit less pronounced as compared to RCP8.5. Also, the interquartile model spread is generally smaller in RCP4.5 and RCP2.6 compared to RCP8.5. Annual and seasonal median increases in TXx generally do not exceed 2°C in RCP2.6 by the end of the century relative to 1981–2000. However, TNn increases

in winter by more than 2°C , even in the lowest forcing scenario RCP2.6, in northern regions such as WNA, CNA, ENA, ALA, GRL, NEU, and NAS.

[34] Frost days particularly decrease in western North America, along the Andes and at the southern tip of South America as well as in central and northern parts of Europe and Asia (Figure 6). The decrease is strongest in RCP8.5 with reductions of 80 frost days and more in northern Europe and western North America by the end of the 21st century.

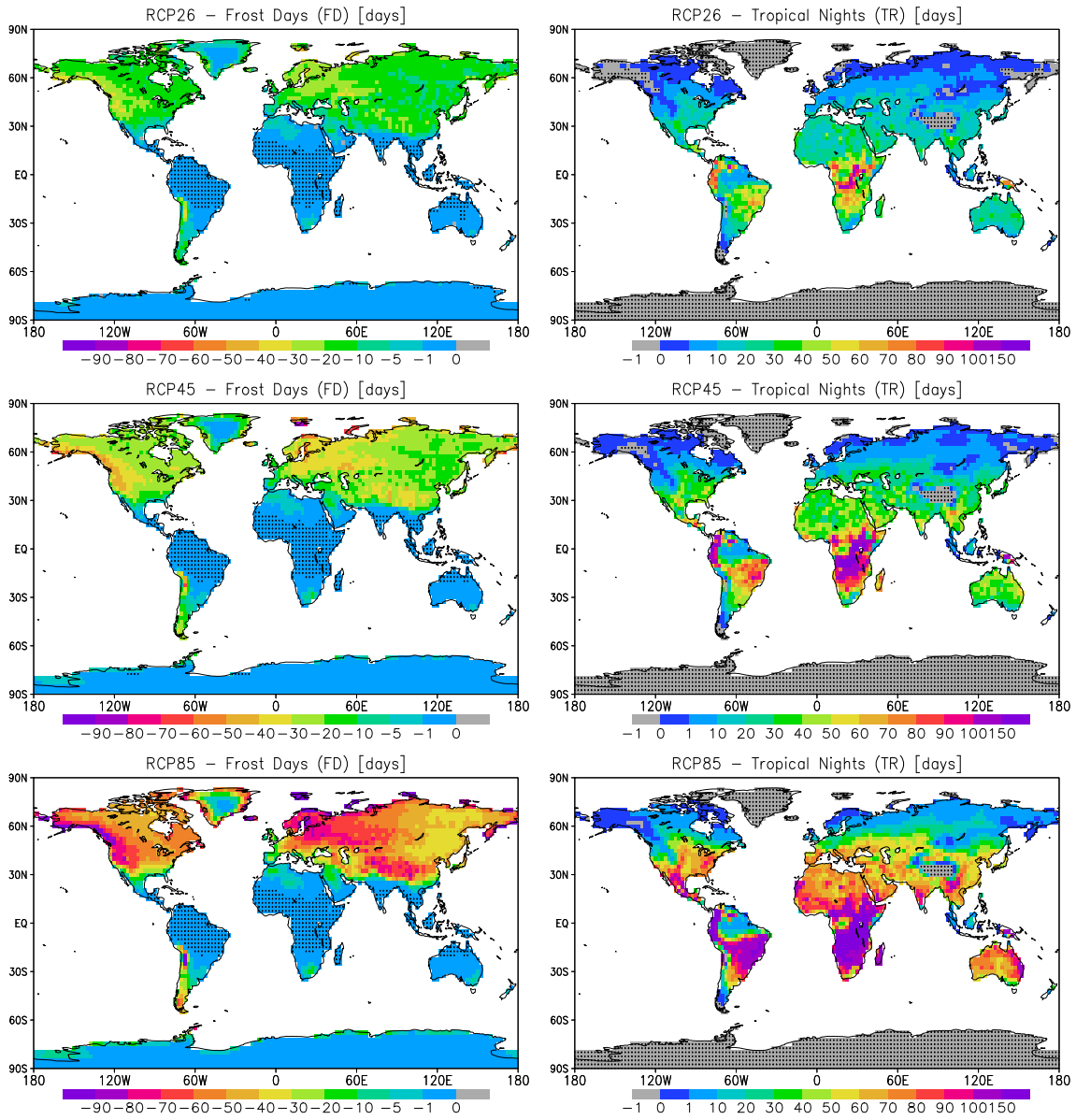


Figure 6. Same as Figure 4, but for frost days (FD, left) and tropical nights (TR, right). Stippling indicates grid points with changes that are not significant at the 5% significance level.

Coastal regions of Antarctica are also projected to experience a significant decrease in FD under all three RCPs.

[35] Tropical nights, based on the fixed 20°C threshold, increase most in tropical regions (>100 days), such as those south of the Amazon, equatorial and southern Africa, and northern Australia (Figure 6). Changes in TR are also relevant for the extra-tropical Northern Hemisphere where nighttime temperatures are currently well below 20°C. Significant increases in TR are seen in the extra-tropical Northern Hemisphere, which are most pronounced in south-eastern North America, the Mediterranean, and central Asia. TR increases by as many as 80 days in these regions under RCP8.5, which would mean that almost the entire summer season will have nighttime temperatures above 20°C. Considering the strong increase in TX_x in the MED and CAS regions as discussed earlier, these regions would face severe heat stress in summer if future climate change follows the path of RCP8.5.

4.1.2. Duration Indices

[36] Consistent with temperature changes described above, cold spell duration (CSDI) is projected to decrease and warm spell duration (WSDI) is projected to increase in all RCPs (Figure 7). The CMIP5 multimodel median changes in these indices are significant everywhere over land. The strongest increases in WSDI occur in tropical regions and are related to the magnitude of the change in mean temperature relative to the low short-term tropical temperature variability. WSDI and CSDI are sensitive to the underlying climatological temperature variability of the respective region [Radinović and Ćurić, 2012], which is small in the tropics and larger in the extra-tropics. Details in the regional changes of CSDI and WSDI under the RCPs can be found in the supporting information (Figure S1).

[37] The temporal evolution of WSDI and CSDI averaged over all land regions is also shown in the supporting information Figure S1. By the end of the 21st century, the median

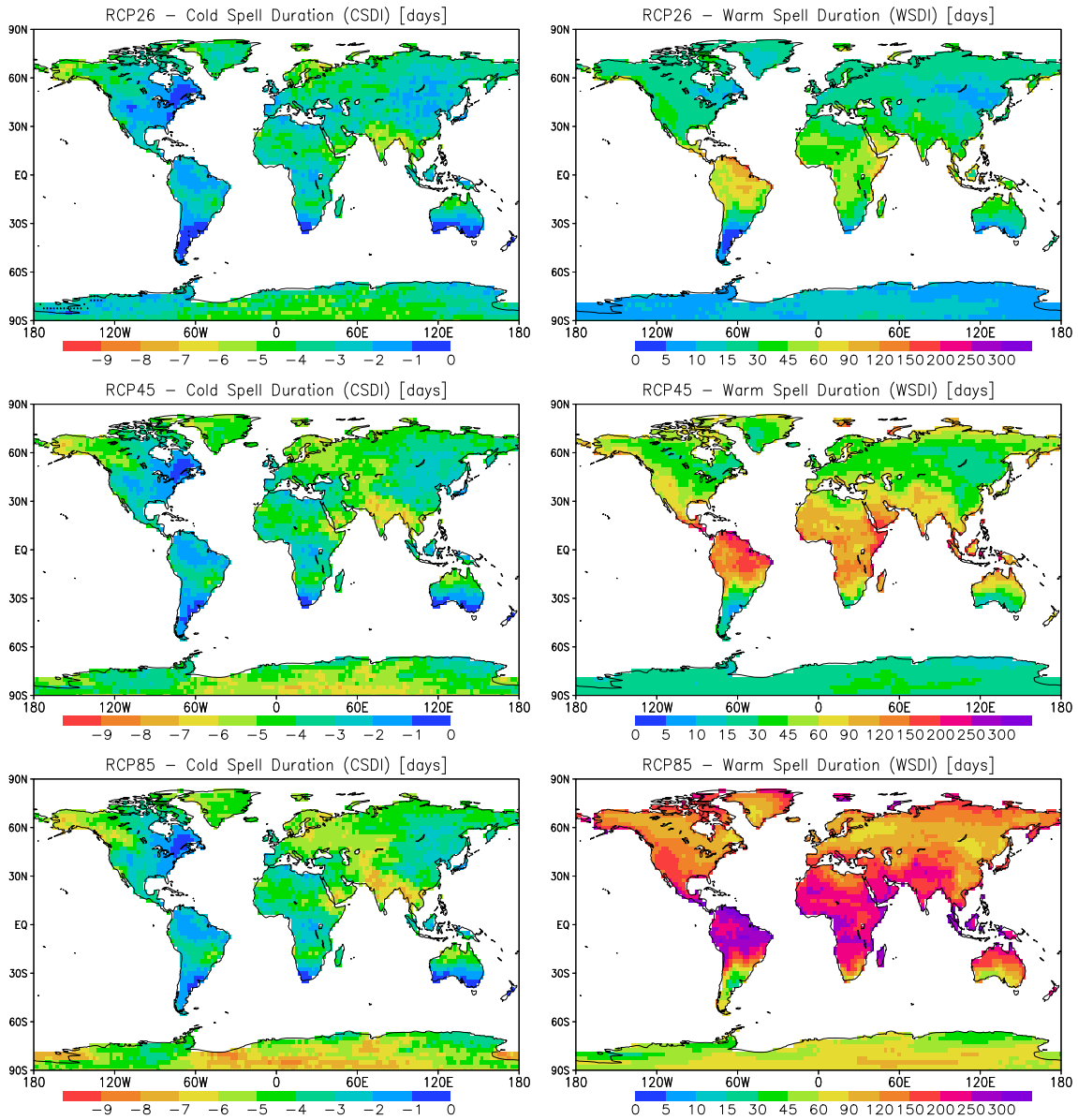


Figure 7. The multimodel median of temporally averaged changes in the cold spell (CSDI, left) and warm spell (WSDI, right) duration index for the period 2081–2100 as differences from the reference period 1981–2000.

CMIP5 models project a decrease in CSDI by about 3.4 days in RCP2.6, 3.9 days in RCP4.5, and 4.2 days in RCP8.5 relative to the 1981–2000 reference period. The projected CMIP3 median decrease in CSDI is somewhat weaker than in the CMIP5 scenarios. WSDI increases strongly under RCP8.5 with about 167 days (globally average over land) by year 2100. The median WSDI increase in RCP4.5 and RCP2.6 is 75 and 31 days, respectively.

4.1.3. Percentile Indices

[38] Projected changes in the percentile indices are shown in absolute terms, and not as differences relative to the reference period as for the other temperature indices. This is because, by construction, the percentile indices represent exceedance rates (in %) relative to the 1961–1990 base period, during which they average to approximately 10%, which will serve as the baseline for future changes.

[39] There is a consistent decrease in cold nights (TN10p) and cold days (TX10p) from the late 20th to the 21st century in all SRES and RCP scenarios (Figures 8a and 8b). The median decrease is generally more pronounced for TN10p than for TX10p. In RCP2.6, TN10p decreases from about 10% in 1961–1990 to 3% by the end of the 21st century and TX10p decreases to 4%. TN10p decreases further to 1.5% in RCP4.5 and 0.3% in RCP8.5, whereas TX10p decreases to 2% and 0.7% in RCP4.5 and RCP8.5 respectively. In the 2046–2065 period, the median changes in SRES B1 are within the RCP2.6 ensemble spread for TN10p and TX10p. For A1B and A2, they are close to the median RCP4.5 change. By the end of the 21st century, the responses for different scenarios diverge further apart, with A2 showing the strongest decrease in TN10p from about 10% to 0.5% and TX10p to 1.3%, which is

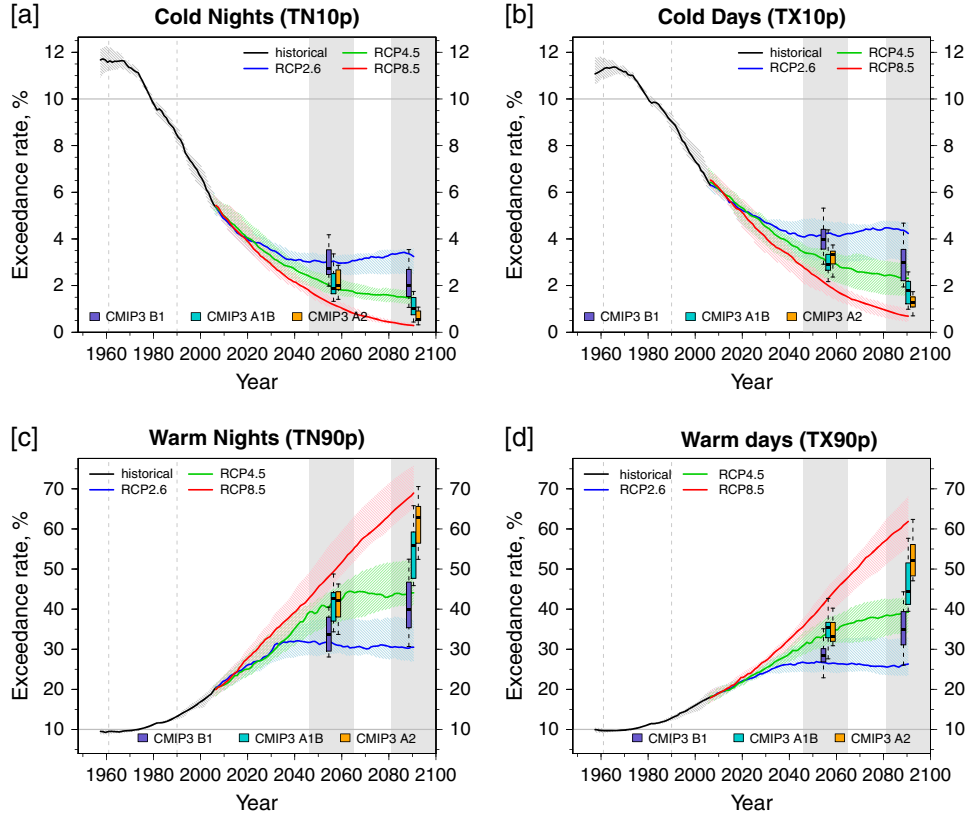


Figure 8. Same as Figure 3, but for the percentile indices (a) cold nights (TN10p), (b) cold days (TX10p), (c) warm nights (TN90p), and (d) warm days (TX90p). Changes are displayed as absolute exceedance rates (in %). By construction the exceedance rate averages to about 10% over the base period 1961–1990.

comparable to the decreases projected under RCP8.5. That is, there will be virtually no cold nights or days as defined for the 1961–1900 base period under these future projections. The decrease of TN10p and TX10p in B1 from about 10% to 2% and to 3%, respectively, is less pronounced than in RCP4.5, whereas TN10p and TX10p decrease to 1% and 2%, respectively, in A1B. The latter changes lie between the RCP4.5 and RCP8.5 projections. The interquartile model spread generally becomes smaller as the projection approaches the zero exceedance rate as more and more models simulate fewer and fewer cold nights and days. Consequently, the largest interquartile model spread is seen for the weaker B1 and RCP2.6 scenarios.

[40] Warm nights and days (TN90p and TX90p, respectively) show a general increase in the exceedance rate toward the end of the 21st century (Figures 8c and 8d). The increase is more pronounced for TN90p than for TX90p. The median increase in TN90p and TX90p in RCP8.5 is from about 10% in 1961–1990 to 69% and 62% by 2100, respectively. The smallest increases in TN90p and TX90p, to 31% and 26% respectively, occur in RCP2.6, followed by greater respective increases to 44% and 39% in RCP4.5. In B1, the median change in TN90p and TX90p is 34% and 29%, respectively, which lies between RCP2.6 and RCP4.5. The A1B median changes are between RCP4.5 and RCP8.5 with increases in TN90p and TX90p, respectively, of 56% and 45%. The median A2 increases in

TN90p and TX90p are from 10% to 63% and 52%, respectively, which is somewhat smaller than in RCP8.5 by 2100.

[41] The simulated decreases in cold days and nights as well as the increases in warm days and nights for the three RCPs are statistically significant everywhere over land (Figure 9 for TN10p and TN90p, and supporting information Figure S2 for TX10p and TX90p). The changes in the percentile indices based on minimum temperature (TN10p and TN90p) are more pronounced than those based on maximum temperature (TX10p and TX90p).

[42] Note that the spatial patterns of change differ from those for the absolute indices TN_n and TX_x. The largest decreases in TN10p and largest increases in TN90p are projected in tropical regions that are characterized by a small day-to-day temperature variability so that changes in mean temperature are associated with comparatively larger changes in exceedance rates below the 10th and above the 90th percentiles. High northern latitudes are also affected by a strong decrease in TN10p in RCP2.6 and RCP4.5. As mentioned before, TN10p decreases to near 0% by year 2100 in most regions under RCP8.5. The smallest changes in the percentile indices, in both TN10p and TN90p, are projected for southern South America.

[43] As pointed out in Klein Tank *et al.* [2009], it is important to interpret changes in percentile indices on a seasonal basis as these indices are calculated relative to the annual cycle of the percentile thresholds. The seasonality

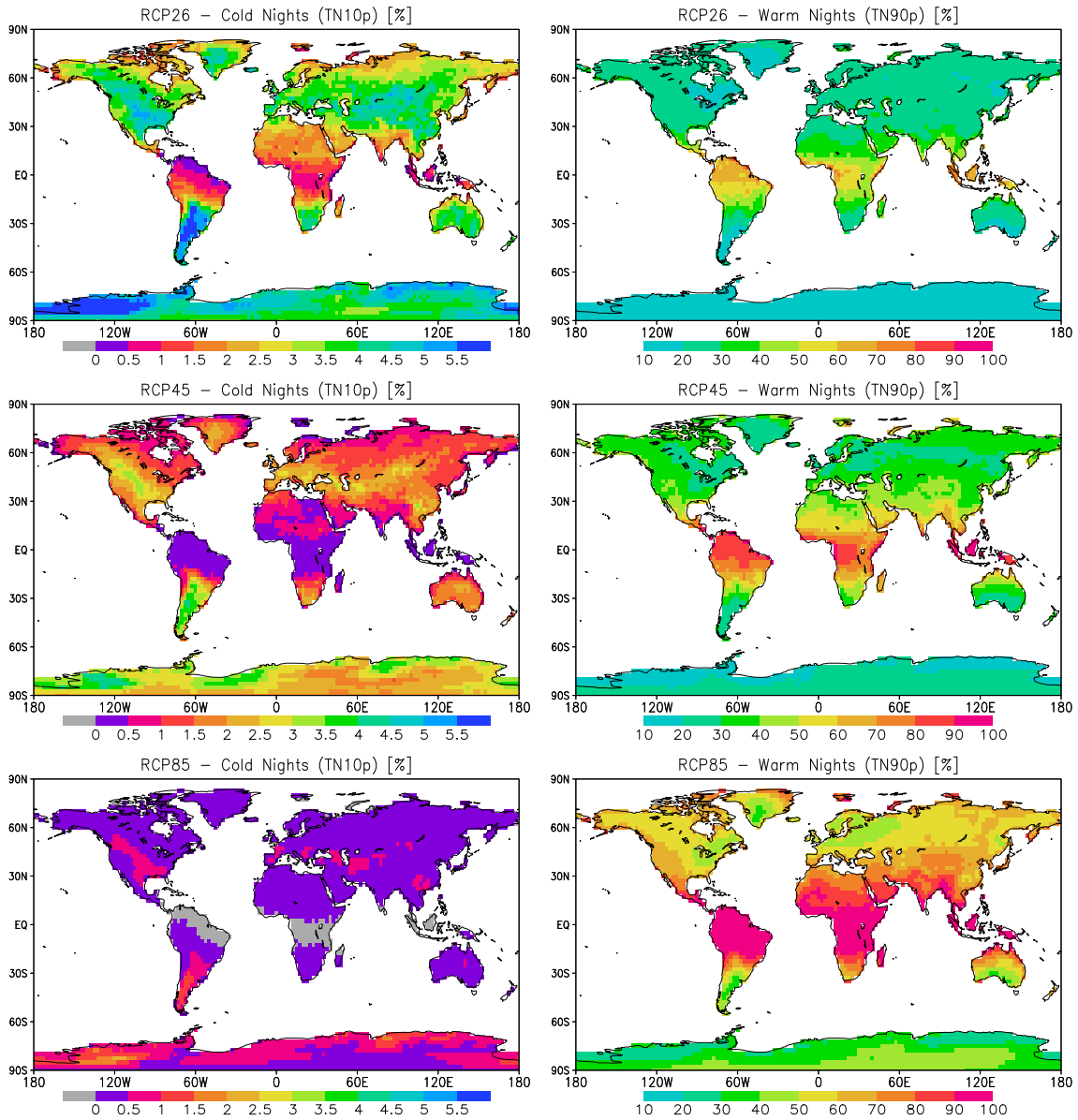


Figure 9. The multimodel median of the annual frequency of cold nights (TN10p, left) and warm nights (TN90p, right) temporally averaged over the period 2081–2100 as absolute values of the exceedance rate (in %). By construction the exceedance rate averages to about 10% over the base period 1961–1990. Gray areas indicate values of exact zero percent. All changes are significant at the 5% significance level.

of changes in the percentile indices by the end of the 21st century is depicted in the box-and-whisker plots in Figure 10. TN10p decreases and TN90p increases most in the summer season (see also supporting information, Figure S3 for seasonal aspects of TX10p and TX90p). This effect is more pronounced in the northern extra-tropics where temperature variability is larger than in the tropics. In JJA, for instance, substantial increases in TN90p (from 10% to 85% in RCP8.5) occur in such regions as MED, EAS, CAS, and TIB. The increase in TN90p in WNA and CNA is twice as large in JJA (~80% exceedance rate) than in DJF (~45% exceedance rate) under RCP8.5. Regions in the Southern Hemisphere, such as AUS and SSA, also show seasonal differences with, for instance, larger increases in TN90p in Southern Hemispheric summer (DJF) compared to winter (JJA).

4.2. Precipitation Indices

4.2.1. Temporal Evolution

[44] Changes in precipitation indices relative to the 1981–2000 reference period are expressed in percentage terms. Global land averaged precipitation indices are projected to increase in the 21st century (Figure 11). Relative increases in RX5day (Figure 11c), which represents a more extreme aspect of the precipitation distribution, are greater over time than those for PRCPTOT and SDII (Figures 11a and 11b). In RCP8.5, PRCPTOT and SDII are projected to increase by 9% and 12%, respectively, by year 2100, whereas RX5day is projected to increase by 20%. PRCPTOT and SDII show similar median increases of about 3.5% in RCP2.6 and somewhat stronger median increases of about 6% in RCP4.5, whereas RX5day increases by 6% and 10% in

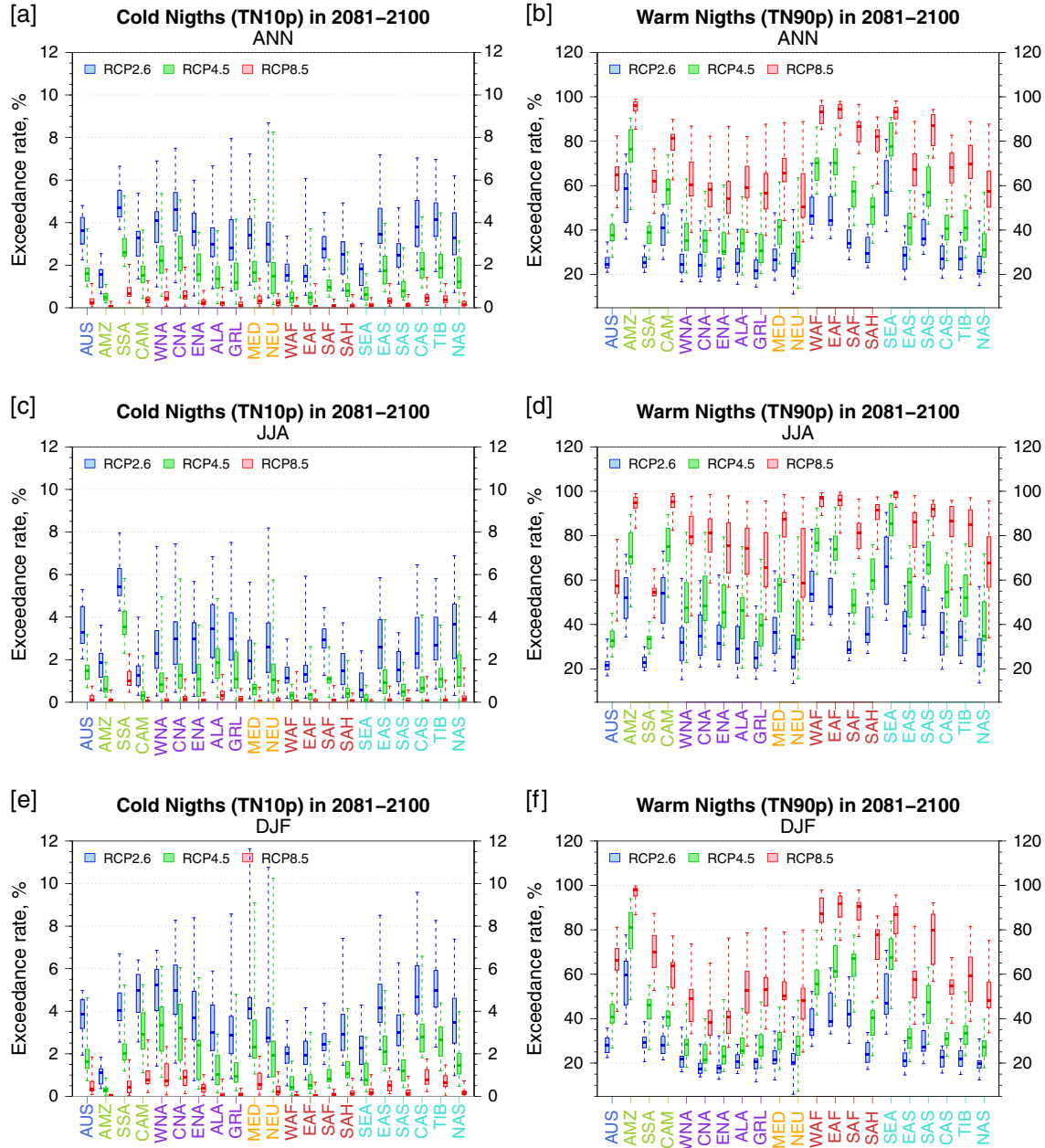


Figure 10. Projected changes in annual, JJA, and DJF frequency of cold nights (TN10p, left) and warm nights (TN90p, right) over the time period 2046–2065 (left) and 2081–2100 (right) for RCP2.6 (blue), RCP4.5 (green), and RCP8.5 (red) as absolute values for the exceedance rate (in %). By construction the exceedance rate averages to about 10% over the base period 1961–1990. Regional mean changes are shown for each of the 21 subregions (cf. Figure 2). Boxes indicate the interquartile model spread of the CMIP5 ensemble with the horizontal line indicating the ensemble median.

RCP2.6 and RCP4.5, respectively. The CMIP5 interquartile model spreads in the three RCPs do not overlap after year 2071 for SDII and RX5day, but remain overlapping for PRCPTOT throughout the 21st century.

[45] The CMIP3 interquartile model spreads in the projection of PRCPTOT, RX5day, and SDII overlap for all three SRES scenarios. The changes in PRCPTOT and SDII range below or around the median response in RCP2.6 for the period 2046–2065. The increase of RX5day under B1 is also comparable to that in RCP2.6, while the median A1B and A2 increase is similar to the RCP4.5 projections.

[46] Toward the end of the 21st century, the median CMIP3 projections for PRCPTOT and SDII diverge more substantially. However, the interquartile model spread also increases and thus the ranges continue to overlap for the three SRES scenarios. By 2100, the median increase in PRCPTOT is 4% in B1, which is between those in RCP2.6 and RCP4.5, 5% in A1B, which is similar to that in RCP4.5, and 6% in A2. SDII increases by 4% in B1, similarly to RCP2.6, and by 5% in A1B, which falls between RCP2.6 and RCP4.5, as does the SDII increase of 7% in A2. For RX5day, the median change of 8% in B1 is between

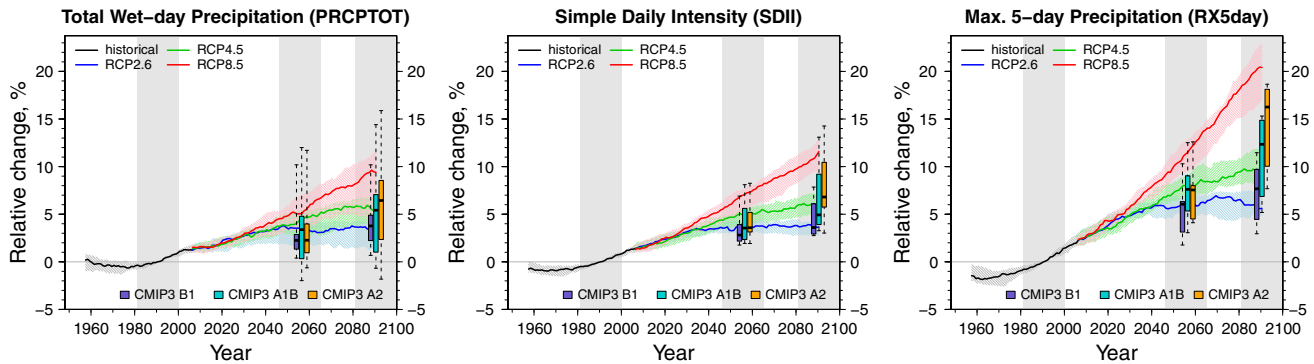


Figure 11. Same as Figure 3, but for precipitation indices. Changes are displayed relative to the reference period 1981–2000 (in %).

RCP2.6 and RCP4.5, whereas the A1B and A2 changes of 12% and 16%, respectively, lie between those in RCP4.5 and RCP8.5. In Sillmann *et al.* [2013], we show that GCMs underestimate observed precipitation magnitudes (e.g., as for RX5day and SDII), although CMIP5 models show an improvement compared to CMIP3. This model bias can be in part attributed to the spatial scale mismatch between point-estimates of precipitation in observations and grid-box-estimates in models. This means that downscaling techniques [e.g., Bürger *et al.*, 2012] should be considered for regional and local assessment of the projected changes in precipitation extremes.

[47] The globally averaged temporal evolution of maximum consecutive dry days (CDD) is not shown here as the temporal and spatial variability of this index over global land is very large (see also Sillmann *et al.*, [2013]). Changes in CDD expressed in terms of global land averages do not provide a meaningful picture, i.e., trends are small as compared to the overall variability in this index. However, changes in this index can be more meaningful for regions where climatic conditions are more uniform as discussed in the following section.

4.2.2. Spatial and Seasonal Patterns of Changes

[48] The ratio of extreme precipitation expressed by very wet days (R95p) to the total wet-day precipitation (PRCPTOT) represents the annual contribution of very wet days to the total annual wet-day precipitation (also referred to as R95pT), which is relevant for societal impacts [Alexander *et al.*, 2006]. Therefore, it is useful to examine changes in PRCPTOT in relation to those in R95p (Figure 12). By the end of the 21st century, PRCPTOT increases significantly over large parts of the Northern Hemisphere, East Africa, South and Southeast Asia as well as Antarctica in all three RCPs relative to the 1981–2000 reference period. The greatest changes are projected in high northern and southern latitudes under RCP8.5. Areas of significant projected decreases in PRCPTOT include Australia (only significant in RCP2.6) as well as South Africa, the Mediterranean region, and Central America (significant in RCP8.5).

[49] Generally, regional increases or decreases in PRCPTOT coincide with corresponding changes in R95p and RX5day (see supporting information Figure S4, right). In particular, R95p increases in high northern latitudes, East Africa, and Antarctica and decreases in Central America, South Africa, and the Mediterranean. The contribution of very wet days to the annual total wet-day precipitation

(expressed by R95pT) generally increases in all three RCPs (see supporting information Figure S4, left).

[50] Regions affected by a decrease in PRCPTOT generally coincide with regions where there is a significant increase in the maximum number of consecutive dry days (CDD) as depicted in Figure 13 (left). In particular, significant increases of CDD occur in Central America, the Mediterranean region as well as southern Africa. The simultaneous decrease in heavy precipitation days (R10mm, Figure 13, right), particular in RCP8.5, indicates an intensification of meteorological drought conditions in these regions. On the contrary, in South and Southeast Asia, the increases in CDD are combined with increases in R10mm and RX5day (see supporting information Figure S4, right) indicating an intensification of both wet and dry seasons in these regions. Significant decreases in CDD are projected at high northern latitudes, Northeast Asia reaching down to the Tibetan Plateau and East Africa as well as Antarctica, which coincide with large increases in R10mm and RX5day in these regions. These regions are projected to become generally wetter in future. The large changes (both CDD increases and decreases) in the Sahara are not significant due to high volatility in the lengths of very long dry spells spanning many years that may occur in this region.

[51] Figure 14 displays regional summaries of annual and seasonal changes in extreme precipitation in terms of RX5day in the 21 subregions. On an annual basis, RX5day generally increases for all three RCPs (Figure 14a). The largest median increase of 30% is projected under RCP8.5 in South Asia (SAS) followed by increases of 20–30% in ALA, GRL, NEU, WAF, EAF, SEA, EAS, TIB, and NAS. In high northern latitude regions, such as ALA, GRL, and NAS, and also in the high altitude TIB region, the increase in RX5day is less pronounced in JJA (Figure 14b) than in DJF (Figure 14c) with the strongest increase in NAS of about 40% in DJF and 20% in JJA. The opposite is seen in SAS, where summer increases are larger than winter increases in RX5day. In SEA and EAS, similar increases in RX5day of about 20% in RCP8.5 are projected for JJA and DJF. Regions for which the CMIP5 ensemble shows no or inconsistent changes in JJA, but an increase in DJF RX5day are AMZ, SSA, WNA, CNA, NEU, and CAS.

[52] The smallest annual increase in RX5day is projected in MED under all three RCPs. In this region, there are large RX5day decreases in summer (JJA), particularly in RCP4.5 and RCP8.5, but only a very small increase (5% or less

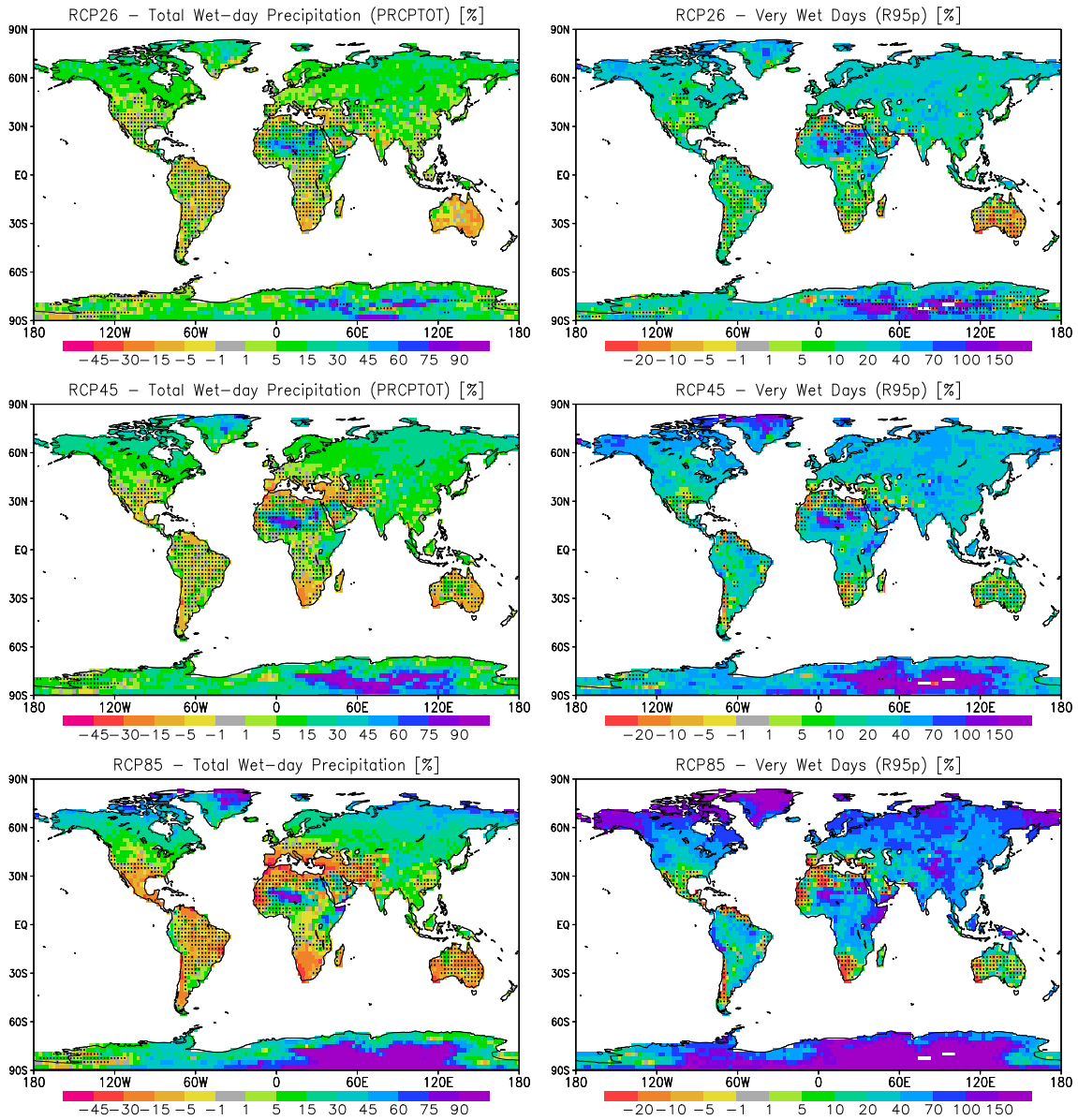


Figure 12. The multimodel median of temporally averaged total wet-day precipitation (PRCPTOT, left), very wet day precipitation (R95p, right) over the time period 2081–2100 expressed relative to the reference period 1981–2000 (in %) for RCP2.6 (top), RCP4.5 (middle), and RCP8.5 (bottom). Stippling indicates grid points with changes that are not significant at the 5% significance level.

depending on the RCP) in winter (DJF). Regions on the Southern Hemisphere, such as AUS and SAF, experience large decreases in RX5day in winter (JJA). In Central America (CAM), RX5day decreases in JJA for most CMIP5 models under RCP8.5 and does so consistently under all RCPs in DJF for the majority of models. These features are not captured in the global maps of annual changes (see supporting information Figure S4, right), where changes in RX5day are not found to be statistically significant in AUS, SAF, and CAM. The decrease of RX5day in combination with the projected increase in CDD (see Figure 13) suggests severe drying of these regions in future climate projections. For regions, such as AMZ, SSA, WNA, CNA, SAH, and CAS, the CMIP5 RX5day projections center around zero in JJA, but show increases in DJF (except SAH). Particularly for

SAH, there is a general disagreement on the sign of seasonal changes in the CMIP5 ensemble with a strong outlier (approximately 113% in ANN and JJA). The model agreement on the sign of changes for precipitation indices is considered in the next section.

4.2.3. Model Agreement

[53] In contrast to the projected changes in the temperature indices, where there is a general agreement on the sign of change independent of the region considered, changes in the precipitation indices are less consistent in this regard. Figure 15 provides a more detailed regional picture of the extent of model agreement on projected changes in the precipitation indices (PRCPTOT, R95p, R10mm, and CDD) over the course of the 21st century. We assess the agreement on the sign of change in the CMIP5 model ensemble on the

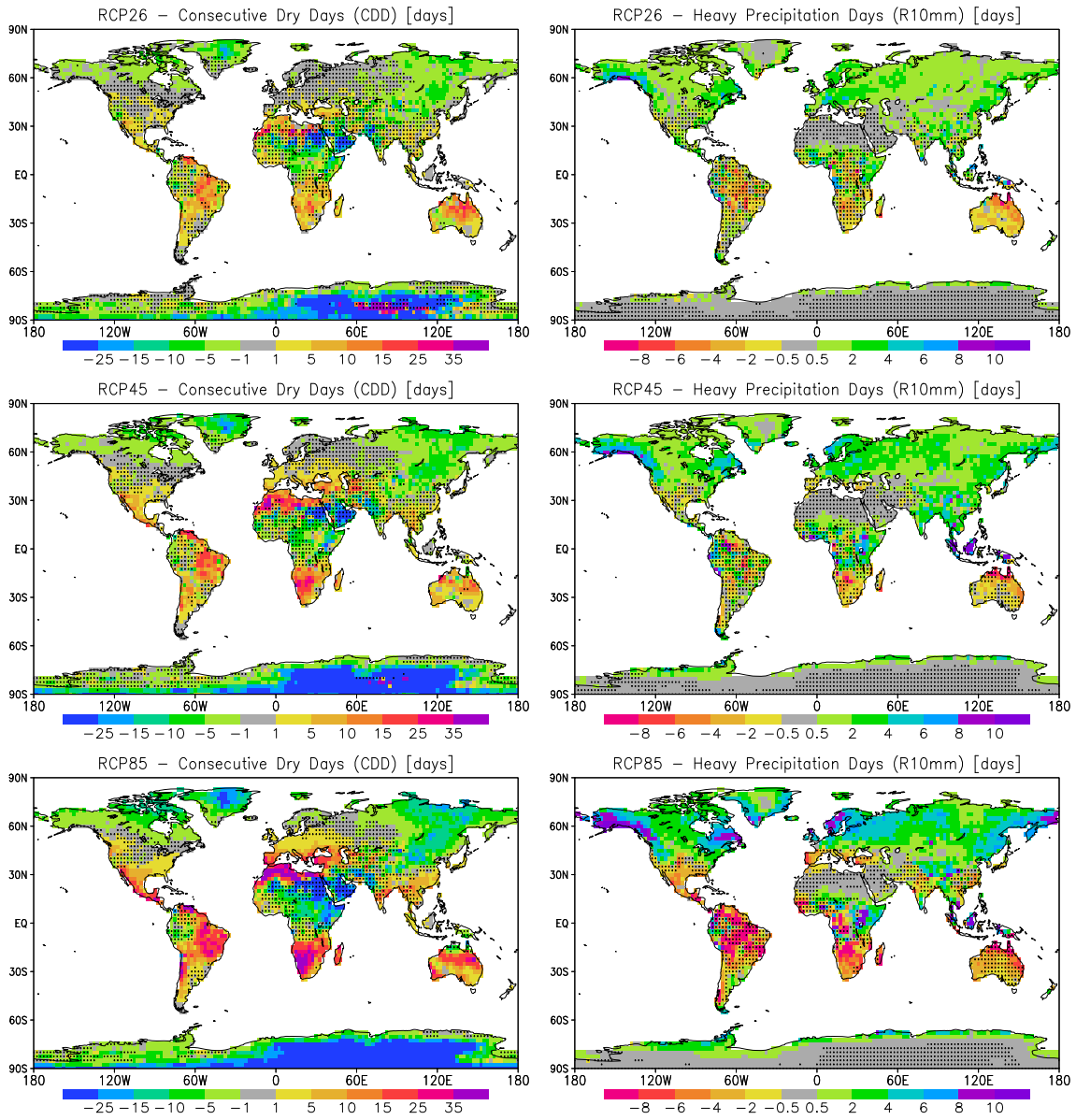


Figure 13. The multimodel median of temporally averaged changes of consecutive dry days (CDD, left) and heavy precipitation days (R10mm, right) over the time period 2081–2100 for RCP2.6 (top), RCP4.5 (middle), and RCP8.5 (bottom). Changes are displayed as differences (in days) relative to the reference period (1981–2000). Stippling indicates grid points with changes that are not significant changes at the 5% significance level.

basis of the interquartile model spread (boxes) for each RCP, which would correspond to an agreement on sign amongst at least 75% of models (referred to as the majority of models in the following), and the full ensemble range (whiskers).

[54] The changes projected for the 2046–2065 period (Figure 15, left column) generally intensify toward the end of the century (right column in Figure 15). Changes in R95p, which represents the more extreme aspects of precipitation variability as compared to the other three indices, are found to be more consistent among the models with most of them generally agreeing on the sign of annual increases across most regions, except AUS, CAM, and SAH. Note that R95p is the only precipitation-based index discussed in this study that is based on the exceedance of a

percentile threshold. It therefore accounts for climatological differences in precipitation between wetter and drier regions [Klein Tank et al., 2009]. The advantages of such an index become particularly obvious in SAH, where the fixed-threshold index R10mm does not indicate any changes since the 10 mm threshold is rarely exceeded in this region, while R95p does show a change.

[55] The PRCPTOT and R10mm show increases in similar regions with the majority of models also agreeing on the sign of the change. These regions comprise WNA, ENA, ALA, GRL, NEU, and all regions in Asia. In the northern high latitude regions (ALA, GRL, and NAS), as well as in TIB and EAS, this increase in precipitation is accompanied by consistent inter-model agreement on a decrease in CDD.

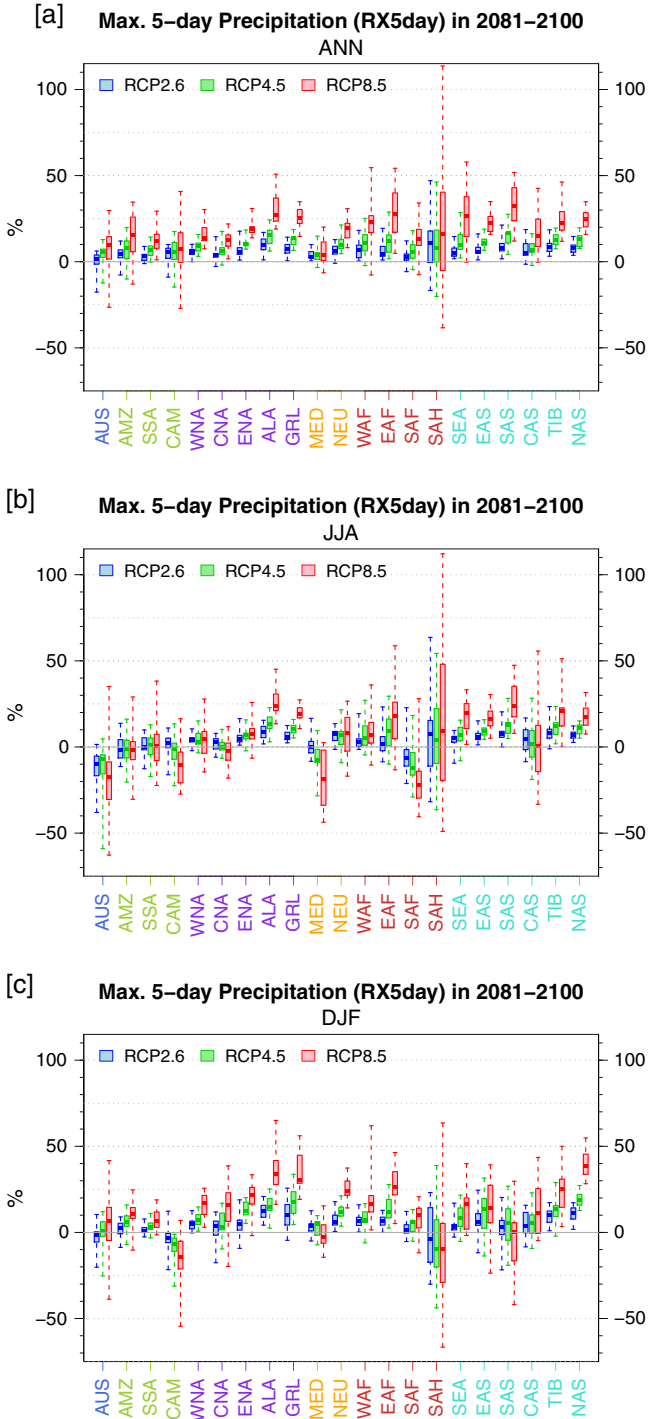


Figure 14. Same as Figure 5, but for projected changes (in %) in annual (ANN), JJA and DJF maximum 5 day precipitation (RX5day) over the time period 2081–2100 relative to the reference period (1981–2000).

In other regions such as WNA, ENA, NEU, SEA, SAS, and CAS, the CMIP5 ensemble projects no consistent change in CDD with models disagreeing on the sign of change for at least one of the three RCPs. Note that the interquartile spread of model changes for regions in northern latitudes is very small compared to regions in the tropics and in the Southern Hemisphere.

[56] The large outliers in the SAH for the precipitation indices PRCPTOT, R95p, are due to the large changes simulated in the model BNU-ESM (with 173% and 468%, respectively). The models MIROC5 and FGOALS-s2 form the extreme outliers in SEA for R10mm with changes of 24% to –11%, respectively.

[57] The majority of CMIP5 models agree on an increase in CDD in AUS, AMZ, SSA, CAM, MED, and SAF under all three RCPs. The strongest increase in CDD toward the end of the 21st century is projected for SAF and MED, followed by AMZ, CAM, and AUS. This increase in CDD coincides with consistent projections by the majority of models of decreases in PRCPTOT and R10mm, particularly in AUS and SAF. In MED, the models disagree on the sign of change in PRCPTOT and R10mm. Depending on the RCP, there are small increases (RCP2.6) or strong decreases (RCP8.5) in PRCPTOT and a tendency for decreases in R10mm with increasing radiative forcing. Note that in regions, such as MED and AMZ, the increases in CDD are accompanied by increases in R95p, suggesting that dry spells in these regions become longer, but that precipitation may be more extreme when it occurs.

[58] The largest interquartile model spread is found for CDD in SAH (Figures 15g and 15h). In this region, the CMIP5 models disagree profoundly on the sign and the magnitude of changes, with outliers (e.g., CDD in IPSL-CM5A-LR and MPI-ESM-LR, respectively, increase by 328 and 297 days in RCP8.5, by 281 and 123 days in RCP4.5, and by 174 and 83 days in RCP2.6). This large range is partly attributed to the large sampling variability associated with dry spells that may span several years. Minor variations in the counts of such long spells in the 20 year time periods considered may result in very large variations of the index.

5. Summary and Concluding Remarks

[59] Projected changes in temperature and precipitation indices defined by the Expert Team of Climate Change Detection and Indices (ETCCDI) are analyzed. The indices are calculated in a consistent manner for the CMIP3 and CMIP5 multimodel ensemble projections of the 21st century for three SRES and three RCP scenarios. The temporal evolution and spatial patterns of changes presented in this study are in agreement with the previous studies by Tebaldi *et al.* [2006] and Orlowsky and Seneviratne [2012]. However, our results are not directly comparable to theirs because a different standardization procedure was applied to the model time series, and because their analysis is in part based on indices whose definitions deviate somewhat from the standard definitions of the ETCCDI.

[60] Results generally indicate an intensification with increasing radiative forcing of patterns of change in temperature- and precipitation-based indices that have already been found in observations [e.g., Frich *et al.*, 2002; Kiktev *et al.*, 2003; Alexander *et al.*, 2006; Min *et al.*, 2010; Morak *et al.*, 2011] and model simulations of the historical climate [Sillmann *et al.*, 2013]. This includes a stronger warming and an increase in precipitation extremes in northern latitudes. In particular, changes in the seasonal minima of TN (TNn) are more pronounced in northern regions where increases are stronger in winter as compared to summer. Strong temperature

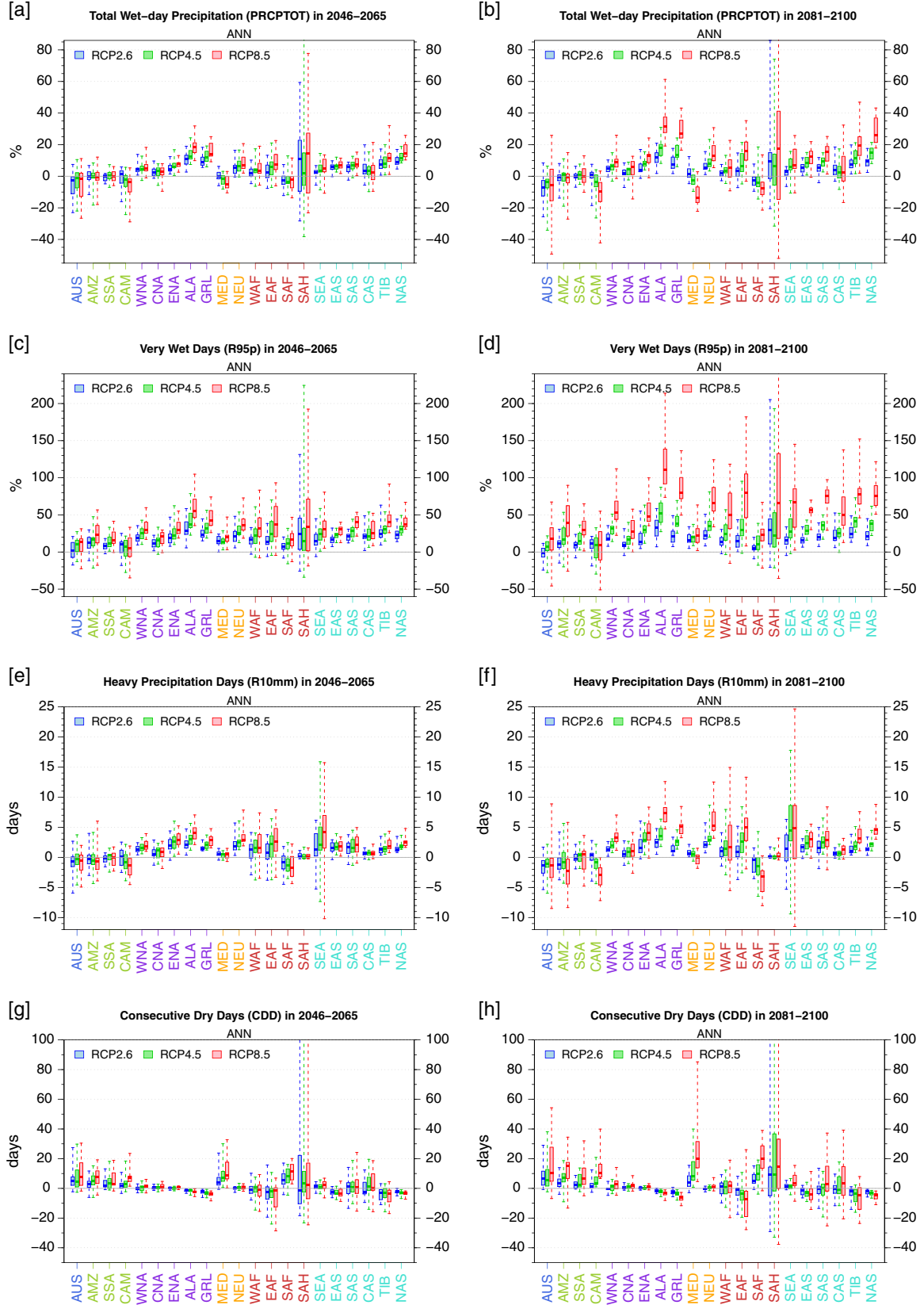


Figure 15. Projected changes in the annual precipitation indices, PRCPTOT, R95p, R10mm, and CDD over two future time periods 2046–2065 and 2081–2100 for RCP2.6 (blue), RCP4.5 (green), and RCP8.5 (red). Regional mean changes are shown for each of the 21 subregions (cf. Figure 2). Boxes indicate the interquartile model spread (25th and 75th quantiles) of the CMIP5 ensemble with the horizontal line indicating the ensemble median. Changes are displayed (in %) for PRCPTOT and R95p and (in days) for R10mm and CDD relative to the reference period 1981–2000.

increases in high northern latitudes have been associated with a number of different mechanisms, including reductions in fall/winter ice and snow cover, indirect responses to decreases in summer ice cover, and increased summer ocean heating as well as changes in the surface heat fluxes [e.g., *Screen and Simmonds*, 2010; *Deser et al.*, 2010; *Flanner et al.*, 2011]. In contrast, changes in the seasonal maxima of TX (TXx) are more uniformly distributed over the global land with generally stronger increases in summer than in winter. Stronger increases in summer TXx also relate to soil-moisture feedbacks as pointed out in *Seneviratne et al.* [2006].

[61] In agreement with previous studies [e.g., *Diffenbaugh and Giorgi*, 2012; *Fischer and Schaer*, 2010; *Giorgi and Lionello*, 2008], the projected changes in the indices stand out in the Mediterranean region indicating a considerable intensification of heat and water stress in that region. The smallest changes in temperature indices are simulated in southern South America, particularly in Southern Hemispheric winter (JJA), in accordance with the small projected changes for the mean temperatures in this region [e.g., *Meehl et al.*, 2007a]. These patterns of climate change intensify with the increasing radiative forcing in the considered scenarios confirming results of previous studies [e.g., *Cubasch et al.*, 1992; *Russo and Sterl*, 2011].

[62] The most notable findings of our study, complementing previous studies, include the following:

[63] • The asymmetry in the warming of minimum and maximum temperatures as observed in the historical record [e.g., *Karl et al.*, 1993; *Trenberth et al.*, 2007] continues and intensifies with increasing radiative forcing in the future climate projections. In particular, projected changes in indices based on TN (warm and cold nights, frost days and tropical nights) are more pronounced than in indices based on TX (e.g., warm and cold days, summer and ice days). Note however that detection and attribution studies based on TN and TX tend to show that models warm TN less than observed and that they warm TX more than observed over the latter half of the 20th century [e.g., *Zwiers et al.*, 2011]. This means, while the contrast in changes between TN and TX in the models corresponds qualitatively with observations, the observed contrast tends to be even larger than simulated by models.

[64] • The spatial patterns of changes in temperature indices depend on the index type. For example, spatial patterns of changes in absolute indices (e.g., TXx and TNn) differ from those in percentile indices. The strongest increase in TNn is in northern high latitudes, whereas changes in TXx are more evenly distributed around the globe. The patterns in TNn and TXx reflect changes that are similar to changes in the mean temperature. In contrast, the percentile indices, such as warm and cold nights, which represent the exceedance rates above or below a percentile threshold derived from the 1961–1990 base period, show the highest increase in the tropical regions where inter-annual temperature variability is relatively small. Therefore, small shifts in the mean of the temperature distribution can lead to larger changes in the exceedance rates than in the high variability extra-tropical regions. Since ecosystems and human infrastructure in the tropics are adapted to relatively small temperature variations, small changes in the extremes can have relatively

large impacts, such as alteration of ecosystems and species extinction [e.g., *Corlett*, 2011].

[65] • Extreme precipitation increases proportionally faster than total wet-day precipitation (PRCPTOT). Changes in very wet days (R95p) indicate that extreme precipitation generally increases in most regions, except for regions such as Australia, Central America, South Africa, and the Mediterranean region where a precipitation decrease and longer dry spells, captured by the consecutive dry days (CDD) index, are projected. The Mediterranean region in particular stands out with an intensification of meteorological drought conditions represented by projected increases in CDD that coincide with decreases in indices describing the wet part of the precipitation distribution, such as heavy precipitation days (R10mm). A slight increase in R95p projected for this region further suggest that although dry conditions become more severe, precipitation can be much more extreme when it does occur.

[66] • Under RCP2.6, with its modest radiative forcing at year 2100, annual global averaged changes in temperature extremes are projected to generally remain below 2°C relative to the reference period 1981–2000. On seasonal and regional scales, however, there are increases in the minimum of TN in winter exceeding 3°C, particularly in northern high latitudes.

[67] • Projected changes in temperature and precipitation extremes are generally more pronounced in RCP4.5 than in B1 simulations, although both have similar amounts of radiative forcing by year 2100. In particular, precipitation extremes under B1 tend to be closer in magnitude to the range of RCP2.6. However, it also has to be kept in mind that CMIP3 and CMIP5 use different sets of GCMs which poses an additional source of uncertainty in making comparisons between SRES and RCP projections. Furthermore, to get a better idea of the changes in extremes in relation to the amount of radiative forcing, other factors (such as aerosol concentrations) that affect climate response would also need to be assessed.

[68] • None of the SRES simulations considered in this study or previous studies (i.e., B1, A1B, and A2) project changes in temperature and precipitation extremes as pronounced as in RCP8.5, which has the largest radiative forcing amongst the scenarios we considered. If greenhouse gas emissions continue to rise at the current pace or even accelerate, very large changes in extremes are to be expected as projected in RCP8.5 simulations.

[69] In conclusion, the different categories of indices (e.g., absolute versus percentile indices) provide complementary information that may be relevant to different applications and a careful selection of indices is necessary. Regional adjustments to the index definitions and sector-based definitions (e.g., for agriculture, drainage and reservoir planning, energy supply, human health, etc.) may be needed to gain more information in individual regions for application in impact and adaptation studies.

[70] Furthermore, future changes in temperature and precipitation extremes need to be assessed carefully in relation to changes in circulation patterns [e.g., *van Oldenborgh et al.*, 2009; *Sillmann and Croci-Maspoli*, 2009] and other feedback mechanisms such as snow, soil moisture, and vegetation [e.g., *Seneviratne et al.*, 2006; *Jaeger and Seneviratne*,

2011; Hirschi *et al.*, 2011]. While this was beyond the scope of this study, it will however be crucial for a comprehensive understanding of the future changes simulated for different regions.

[71] Additional work will also be required to better quantify the uncertainties in the projected changes in the indices. The model spread and variations in response to the different SRES and RCP scenarios are indicative of uncertainties associated with natural internal variability of the climate system, structural, and parametric uncertainty as embodied by the range of climate models considered, and future forcing uncertainty. Not considered here, but equally important, is observational and process knowledge uncertainty, as represented by differences between observational and observationally constrained analyses (i.e., reanalyses) and differences between models in replicating the climatological behavior of the indices in the recent past as documented in Part I of this paper [Sillmann *et al.*, 2013]. While most models represent extremes reasonably well, including trends in the present climate, it should be noted that there are also some indices, which are not well represented or difficult to evaluate with currently available observational datasets (e.g., SDII and diurnal temperature range (DTR)).

[72] The results presented in this study give a first impression of what we can expect from the new CMIP5 multimodel ensemble and subsequent studies will no doubt provide more insights into seasonal and regional changes. As the complete set of indices calculated across the CMIP3 and CMIP5 ensembles as well as the SRES and RCP scenarios will be provided on the ETCCDI indices archive (<http://www.cccma.ec.gc.ca/data/climdex/climdex.shtml>), we hope to encourage further studies of the changes in climate extremes and to facilitate impact studies and the development of adaptation strategies by providing the necessary physical basis.

[73] **Acknowledgments.** We acknowledge the World Climate Research Programme's Working Group on Coupled Modelling, which is responsible for CMIP, and we thank the climate modeling groups (listed in Tables 1 and 2 of this paper) for producing and making available their model output. For CMIP, the U.S. Department of Energy's Program for Climate Model Diagnosis and Intercomparison provides coordinating support and led development of software infrastructure in partnership with the Global Organization for Earth System Science Portals. F.Z. is supported by Australian Research Council (grant LP100200690) and J.S. is funded by the German Research Foundation (grant Si 1659/1-1). We thank Greg Flato, Chris Derksen, Ross Brown and Elizabeth Bush, and three reviewers for their helpful comments on the manuscript.

References

- Alexander, L., et al. (2006), Global observed changes in daily climate extremes of temperature and precipitation, *J. Geophys. Res.*, **111**, D05109, doi:10.1029/2005JD006290.
- Bürger, G., T. Q. Murdock, A. T. Werner, S. R. Sobie, and A. J. Cannon (2012), Downscaling extremes—An intercomparison of multiple statistical methods for present climate, *J. Climate*, **25**, 4366–4388, doi:10.1175/JCLI-D-11-00408.1.
- Cardona, O., M. van Aalst, J. Birkmann, M. Fordham, G. McGregor, R. Perez, R. Pulwarty, E. Schipper, and B. Sinha (2012), Determinants of risk: Exposure and vulnerability, in *Managing the Risks of Extreme Events and Disasters to Advance Climate Change Adaptation. A Special Report of Working Groups I and II of the Intergovernmental Panel on Climate Change (IPCC)*, pp. 65–108, Cambridge University Press, Cambridge, UK, and New York, NY, USA.
- Corlett, R. T. (2011), Impacts of warming on tropical lowland rainforests, *Trends Ecol. Evol.*, **26**, 606–613, doi:10.1016/j.tree.2011.06.015.
- Cubasch, U., K. Hasselmann, H. Höck, E. Maier-Reimer, U. Mikolajewicz, B. Santer, and R. Sausen (1992), Time-dependent greenhouse warming computations with a coupled ocean-atmosphere model, *Clim. Dyn.*, **8**, 55–69.
- Deser, C., R. Tomas, M. Alexander, and D. Lawrence (2010), The seasonal atmospheric response to projected Arctic sea ice loss in the late twenty-first century, *J. Climate*, **23**, 333–351, doi:10.1175/2009JCLI3053.1.
- Diffenbaugh, N. S., and F. Giorgi (2012), Climate change hotspots in the CMIP5 global climate model ensemble, *Clim. Chang.*, **114**, 813–822, doi:10.1007/s10584-012-0570-x.
- Fischer, E. M., and C. Schaer (2010), Consistent geographical patterns of changes in high-impact European heatwaves, *Nat. Geosci.*, **3**, 398–403, doi:10.1038/ngeo866.
- Flanner, M. G., K. M. Shell, M. Barlage, D. K. Perovich, and M. A. Tschudi (2011), Radiative forcing and albedo feedback from the Northern Hemisphere cryosphere between 1979 and 2008, *Nat. Geosci.*, **4**, 151–155, doi:10.1038/ngeo1062.
- Frich, P., L. Alexander, P. Della-Marta, B. Gleason, M. Haylock, A. Klein Tank, and T. Peterson (2002), Observed coherent changes in climate extremes during the second half of the twentieth century, *Clim. Res.*, **19**, 193–212, doi:10.3354/cr019193.
- Giorgi, F., and R. Francisco (2000), Uncertainties in regional climate change prediction: A regional analysis of ensemble simulations with the HADCM2 coupled AO/GCM, *Clim. Dyn.*, **16**, 169–182.
- Giorgi, F., and P. Lionello (2008), Climate change projections for the Mediterranean region, *Global Planet. Chang.*, **63**, 90–104, doi:10.1016/j.gloplacha.2007.09.005.
- Gleckler, P. J., K. E. Taylor, and C. Doutriaux (2008), Performance metrics for climate models, *J. Geophys. Res.*, **113**, D06104, doi:10.1029/2007JD008972.
- Hirschi, M., S. Seneviratne, V. Alexandrov, F. Boberg, C. Boroneanț, O. Christensen, H. Formayer, B. Orlowsky, and P. Stepanek (2011), Observational evidence for soil-moisture impact on hot extremes in southeastern Europe, *Nat. Geosci.*, **4**, 17–21, doi:10.1038/ngeo1032.
- IPCC (2007), *Climate Change 2007: The Physical Science Basis. Contribution of Working Group I to the Fourth Assessment Report of the Intergovernmental Panel on Climate Change*, pp. 996, Cambridge University Press, Cambridge, UK and New York, NY, USA.
- IPCC (2012), *Managing the Risks of Extreme Events and Disasters to Advance Climate Change Adaptation. A Special Report of Working Groups I and II of the Intergovernmental Panel on Climate Change*, pp. 582, Cambridge University Press, Cambridge, UK, and New York, NY, USA.
- Jaeger, E. B., and S. I. Seneviratne (2011), Impact of soil moisture-atmosphere coupling on European climate extremes and trends in a regional climate model, *Clim. Dyn.*, **36**, 1919–1939, doi:10.1007/s00382-010-0780-8.
- Karl, T. R., et al. (1993), Asymmetric trends of daily maximum and minimum temperature, *Papers in Natural Resources, Paper 185*.
- Kharin, V. V., F. W. Zwiers, X. Zhang, and G. C. Hegerl (2007), Changes in temperature and precipitation extremes in the IPCC ensemble of global coupled model simulations, *J. Climate*, **20**, 1419–1444, doi:10.1175/JCLI4066.1.
- Kiktev, D., D. M. H. Sexton, L. Alexander, and C. K. Folland (2003), Comparison of modeled and observed trends in indices of daily climate extremes, *J. Climate*, **16**, 3560–3571, doi:10.1175/1520-0442(2003)016<3560:COMAOT>2.0.CO;2.
- Klein Tank, A. M. G., F. W. Zwiers, and X. Zhang (2009), Guidelines on analysis of extremes in a changing climate in support of informed decisions for adaptation, *Climate data and monitoring WCDMP-No. 72, WMO-TD No. 1500*, 56pp.
- Meehl, G., et al. (2007a), Global climate projections, in *Climate Change 2007: The Physical Science Basis. Contribution of Working Group I to the Fourth Assessment Report of the Intergovernmental Panel on Climate Change*, Cambridge University Press, Cambridge, United Kingdom and New York, NY, USA, 747–846.
- Meehl, G. A., C. Covey, T. Delworth, M. Latif, B. McAvaney, J. F. B. Mitchell, R. J. Stouffer, and K. E. Taylor (2007b), The WCRP CMIP3 multi-model dataset: A new era in climate change research, *Bull. Am. Meteorol. Soc.*, **88**, 1383–1394.
- Min, S.-K., X. Zhang, F. W. Zwiers, and G. C. Hegerl (2010), Human contribution to more-intense precipitation extremes, *Nature*, **470**, 378–381, doi:10.1038/nature09763.
- Morak, S., G. C. Hegerl, and J. Kenyon (2011), Detectable regional changes in the number of warm nights, *Geophys. Res. Lett.*, **38**, L17703, doi:10.1029/2011GL048531.
- Moss, R. H., et al. (2010), The next generation of scenarios for climate change research and assessment, *Nature*, **463**, 747–756, doi:10.1038/nature08823.
- Mueller, B., and S. I. Seneviratne (2012), Hot days induced by precipitation deficits at the global scale, *Proc. Natl. Acad. Sci. (USA)*, *PNAS Early Edition*, 6 pp. doi:10.1073/pnas.1204330109.

- Nakicenovic, N., et al. (2000), Special Report on Emission Scenarios, pp. 612, Cambridge University Press, Cambridge, UK, ISBN 0521804930.
- Orlowsky, B., and S. I. Seneviratne (2012), Global changes in extreme events: Regional and seasonal dimension, *Clim. Chang.*, **110**, 669–696, doi:10.1007/s10584-011-0122-9.
- Patz, J. A., D. Campbell-Lendrum, T. Holloway, and J. A. Foley (2005), Impact of regional climate change on human health, *Nat. Rev.*, **438**, 310–317, doi:10.1038/nature04188.
- Power, S. B., F. Delage, R. Colman, and A. Moise (2012), Consensus on twenty-first-century rainfall projections in climate models more widespread than previously thought, *J. Climate*, **25**, 3792–3809, doi:10.1175/JCLI-D-11-00354.1.
- Radinović, D., and M. Ćurić (2012), Criteria for heat and cold wave duration indexes, *Theor. Appl. Climatol.*, **107**, 505–510, doi:10.1007/s00704-011-0495-8.
- Riahi, K., S. Rao, V. Krey, C. Cho, V. Chirkov, G. Fischer, G. Kindermann, N. Nakicenovic, and P. Rafaj (2011), RCP8.5—A scenario of comparatively high greenhouse gas emissions, *Clim. Chang.*, **109**, 33–57, doi:10.1007/s10584-011-0149-y.
- Rogelj, J., M. Meinshausen, and R. Knutti (2012), Global warming under old and new scenarios using IPCC climate sensitivity range estimates, *Nat. Clim. Chang.*, **2**, 248–253, doi:10.1038/nclimate1385.
- Russo, S., and A. Sterl (2011), Global changes in indices describing moderate temperature extremes from the daily output of a climate model, *J. Geophys. Res.*, **116**, D03104, doi:10.1029/2010JD014727.
- Screen, J. A., and I. Simmonds (2010), Increasing fall-winter energy loss from the Arctic Ocean and its role in Arctic temperature amplification, *Geophys. Res. Lett.*, **37**, L16707, doi:10.1029/2010GL044136.
- Seneviratne, S. I., D. Lüthi, M. Litschi, and C. Schäer (2006), Land-atmosphere coupling and climate change in Europe, *Lett. Nat.*, **443**, 205–209, doi:10.1038/nature05095.
- Sillmann, J., and M. Croci-Maspoli (2009), Present and future atmospheric blocking and its impact on European mean and extreme climate, *Geophys. Res. Lett.*, **36**, L10702, doi:10.1029/2009GL038259.
- Sillmann, J., and E. Roeckner (2008), Indices for extreme climate events in projections of anthropogenic climate change, *Clim. Chang.*, **83**–104, doi:10.1007/s10584-007-9308-6.
- Sillmann, J., V. V. Kharin, X. Zhang, F. W. Zwiers, and D. Bronaugh, (2013), Climate extremes indices in the CMIP5 multimodel ensemble: Part 1. Model evaluation in the present climate, *J. Geophys. Res. Atmos.*, **118**, 1–18, doi:10.1002/jgrd.50203.
- Taylor, K. E., R. J. Stouffer, and G. A. Meehl (2012), An overview of CMIP5 and the experiment design, *Bull. Am. Meteorol. Soc.*, **93**, 485–498, doi:10.1175/BAMS-D-11-00094.1.
- Tebaldi, C., K. Hayhoe, J. Arblaster, and G. Meehl (2006), Going to extremes. An intercomparison of model-simulated historical and future changes in extreme events, *Clim. Chang.*, **79**, 185–211, doi:10.1007/s10584-006-9051-4.
- Tebaldi, C., J. M. Arblaster, and R. Knutti (2011), Mapping model agreement on future climate projections, *Geophys. Res. Lett.*, **38**, L23701, doi:10.1029/2011GL049863.
- Terando, A., K. Keller, and W. E. Easterling (2012), Probabilistic projections of agro-climate indices in North America, *J. Geophys. Res.*, **117**, D08115, doi:10.1029/2012JD017436.
- Thomson, A. M., et al. (2011), RCP4.5: A pathway for stabilization of radiative forcing by 2100, *Clim. Chang.*, **109**, 77–94, doi:10.1007/s10584-011-0151-4.
- Trenberth, K., et al. (2007), Observations: Surface and atmospheric climate change, in *Climate Change 2007: The Physical Science Basis. Contribution of Working Group I to the Fourth Assessment Report of the Intergovernmental Panel on Climate Change*, Cambridge University Press, Cambridge, United Kingdom and New York, NY, USA, 235–336.
- van Oldenborgh, G. J., S. Drijfhout, A. van Ulden, R. Haarsma, A. Sterl, C. Severijns, W. Hazleger, and H. Dijkstra (2009), Western Europe is warming much faster than expected, *Clim. Past*, **5**, 1–12, doi:10.5194/cp-5-1-2009.
- van Vuuren, D. P., et al. (2011a), RCP2.6: Exploring the possibility to keep global mean temperature increase below 2°C, *Clim. Chang.*, **109**, 95–116, doi:10.1007/s10584-011-0152-3.
- van Vuuren, D. P., et al. (2011b), The representative concentration pathways: An overview, *Clim. Chang.*, **109**, 5–31, doi:10.1007/s10584-011-0148-z.
- Weisskopf, M. G., H. A. Anderson, S. Foldy, L. P. Hanrahan, K. Blair, T. J. Trk, and P. D. Rumm (2002), Heat wave morbidity and mortality, Milwaukee, Wis, 1999 vs 1995: An improved response?, *Am. J. Public Health*, **92**, 830–833.
- Wilks, D. S. (2006), *Statistical Methods in the Atmospheric Sciences*, 2nd edition, Academic Press, San Diego, 648.
- Zhang, X., G. Hegerl, F. Zwiers, and J. Kenyon (2005), Avoiding inhomogeneity in percentile-based indices of temperature extremes, *J. Climate*, **16**41–1651, doi:10.1175/JCLI3366.1.
- Zhang, X., L. Alexander, G. C. Hegerl, P. Jones, A. K. Tank, T. C. Peterson, B. Trewin, and F. W. Zwiers (2011), Indices for monitoring changes in extremes based on daily temperature and precipitation data, *WIREs Clim. Chang.*, **2**, 851–870, doi:10.1002/wcc.147.
- Zwiers, F., X. Zhang, and Y. Feng (2011), Anthropogenic influence on long return period daily temperature extremes at regional scales, *J. Climate*, **24**, 881–892, doi:10.1175/2010JCLI3908.1.